Analysis of Spinal Rod Deformation After Cutting with a Surgical Rod Cutter

James Egan
B.S., University of Iowa, IA, 2021
Submitted to the graduate degree program in Bioengineering and the Graduate Faculty of the University of Kansas in partial fulfillment of the requirements for the degree of Master of Science.

_____

Chair: Dr. Elizabeth Friis

_____

Dr. Lorin Maletsky

_____

Dr. Terrence McIff

Date Defended: 17 August, 2023

The thesis committee for James Egan certifies that this is the
approved version of the following thesis:
Analysis of Spinal Rod Deformation After Cutting with a Surgical Rod Cutter

_____

Chair: Dr. Lisa Friis

Date Approved: 5 September, 2023

Abstract

Scoliosis, a deformity characterized by an abnormal curvature of the spine, requires various treatment approaches depending on the severity of the condition, including surgical or non-surgical options. Surgical procedures, often involving the use of spinal fusion rods, play a crucial role in correcting spinal deformities. However, the process of cutting these rods with a surgical rod cutter may introduce deformations at the cut ends, potentially leading to complications and compromised treatment outcomes.

This paper presents an analysis of the deformation observed in scoliosis rods after they have been cut using a surgical rod cutter. Identification of the extent and characteristics of deformations that occur during the cutting process will be assessed, as well as determining the point at which deformation ceases along the length of the rods.

To achieve this objective, photogrammetry and three-dimensional modeling techniques were employed. Photogrammetry was used to create accurate three-dimensional models of these rods from two-dimensional photographs, providing a detailed representation of the deformed rod ends. Precise measurements and analysis were then performed to quantify and characterize the deformations.

Three different diameters (4.75mm, 5.5mm, and 6.0mm) of two different types of metal rods (Titanium and Cobalt Chrome) resulting in six different experimental groups, were analyzed. Analysis of the deformed rod ends involved assessing the deviating angle of the plasticly deformed region of the rod and the roundness of the deformed cross sections. The higher diameter the rod, the more deformation was experienced. Cobalt chrome also experienced more angular deviation and lower roundness compared to its Titanium counterpart. Once all angular deviations reached 0 degrees and roundness values reached above 0.985, there was

confidence there was minimal deformation at that spot. For the 4.75 mm and 5.5 mm Ti rods, 4 mm of space is required between the edge of the cut to where there is minimal deformation. For the 6.0 mm Ti, and all CoCr rods, 5 mm of space is needed. These data remain consistent with metal deformation studies, which show larger diameter rods deforming more than smaller ones, as well as CoCr deforming more than Ti. It is crucial to leave the required room to decrease the chances of instrument failure.

This study contributes to the ongoing improvement of surgical techniques and treatment outcomes in scoliosis management. The analysis of deformation in scoliosis rods after cutting provides important information for optimizing surgical procedures and enhancing the long-term success of spinal fusion treatments.

Acknowledgments

Dr. Lisa Friis

Dr. Friis, thank you for allowing me to be a part of your lab and your continued guidance. I believe I have grown a lot as an engineer and a scientist here at KU and a big part of that is through what you have taught me.

Dr. Maletsky and Dr. McIff

Thank you both for agreeing to be a part of my committee and being supportive and helpful in my time here at KU. I have truly enjoyed working with both of you over the last few years.

Dr. Anderson, Dr. Schwend, and Dr. Erickson

Thank you for this opportunity and all your support over the last couple of years. I have enjoyed working with you all and everyone else over at CMH.

The Friis Lab

To my lab mates: Tori Drapal, Savannah Mosier, Jordan Gamble, Chris Tacca, Josh Dugdale, and Morgan Riley, I can't thank you all enough for the constant support you've shown me over the last few years. I am very blessed to have such an incredible group of people by my side. Thank you for the connections you have brought me and the memories we have shared. I will never forget it.

My Family and Friends

To my family and friends, thank you for always supporting and believing in me, and when I needed it, making me forget about grad school briefly. I couldn't have done this without all of you either.

Table of Contents

List of Figures

List of Tables

List of Abbreviations

CRP	Close-Range Photogrammetry
CT	Computed Tomography
MCGR	Magnetically Controlled Growing Rods
OR	Operating Room
TGF- β	Transforming Growth Factor-Beta
UAV	Unmanned Aerial Vehicle
VBS	Vertebral Body Stapling
VBT	Vertebral Body Tethering
VDR	Vitamin D Receptor
VEPTR	Vertebral Expansion Prosthetic Titanium Rib

List of Equations

Chapter 1: Introduction

1.1 Introduction and Motivation

Scoliosis has been broadly defined as irregular curvature of the spine. Many side effects come from the existence of scoliosis in a patient, including cardiopulmonary symptoms, chronic back pain, and an altered appearance (1). Any patient may develop scoliosis, but it is significantly more common in children and adolescents under 18. For most scoliosis cases, the true cause of the disease is unknown. However, there are some common causes that have been identified and linked to the disease. These causes may include birth defects, injury, and genetic disorders, among others.

Treatment for the affected can be through non-invasive or invasive surgical approaches. If the disease is caught early enough in children, typically doctors will stick to non-invasive approaches until the patient absolutely needs a procedure done. If the patient needs an operative treatment, there are three categories of options: distraction-based, compression-based, and growth guided (2). The most common technique used to correct spinal curvature is using spinal fusion rods. Currently, titanium and cobalt-chrome alloys are the most common materials used in these rods.

Spinal fusion rods are used in instances where there is not expected to be much more growth or development in the patient, so they are typically used in adolescents, whereas growing rods are used in children under 10. These spinal fusion rods are not manufactured on a case-by-case basis. Rather, they are cut with a rod cutter in the operating room (OR) after taking measurements. However, due to the force of the rod cutter, during cutting a small amount of plastic deformation forms at the end of the remaining rod. This permanent deformation may hinder the ability of the rod to sit correctly in its corresponding pedicle screw as they are precisely manufactured. This may lead to several potential complications including reduced stability, rod

dislodgement, implant failure, pain, and revision surgeries (7,45,51). Therefore, the purpose of this work was to analyze and measure the profile of the deformed end of the rod once they have been subject to the rod cutter and determine at what point there is no deformation in the rod.

Photogrammetry was used to create three-dimensional models of the deformed end of the rod. Photogrammetry is the creation of three-dimensional models from two-dimensional photographs. With current computer and camera technology, photogrammetry is redefining the ability to acquire, analyze, and utilize spatial data. Accurate measurements can be recorded with this technology. In experiments where the subject is small (tooth sized), dimensions accurate to tenths of a millimeter can be measured (34). And in larger objects, such as an airplane wing, measurement errors are as low as 1.25% (33).

Chapter 2. Background and Literature Review

2.1 Scoliosis

Scoliosis is defined as an irregular curvature of the spine and occurs in approximately 1-3% of the US population (7,8). There are different severities of structural or rotational irregularities that may contribute to the overall health of the patient and result in different classifications of scoliosis patients. The irregularities can be classified into three broad types, based on their respective etiology; idiopathic, neuromuscular, and congenital (4). Idiopathic scoliosis describes a situation where the cause of the disease is largely unknown, so both genetic and hereditary factors are considered in these scenarios. Idiopathic scoliosis is the most common form of scoliosis, found in approximately 80% of all cases (6). Neuromuscular scoliosis is used to classify patients that develop scoliosis as a consequence of another neurological disease (35). Such diseases include cerebral palsy, muscle fiber disorders, or spinal cord injury. Neuromuscular scoliosis is typically more severe and progressive and has a higher morbidity rate associated with it. Congenital scoliosis occurs when the deformity is present at birth and occurs in roughly 1 of every 1000 live births (36). Treatment for patients with this condition may be different from the other disease types as treatment plans begin at birth. An example of what this looks like in a patient can be seen in Figure 1. Figure 1 displays a representative image of what scoliosis may look like in the body.

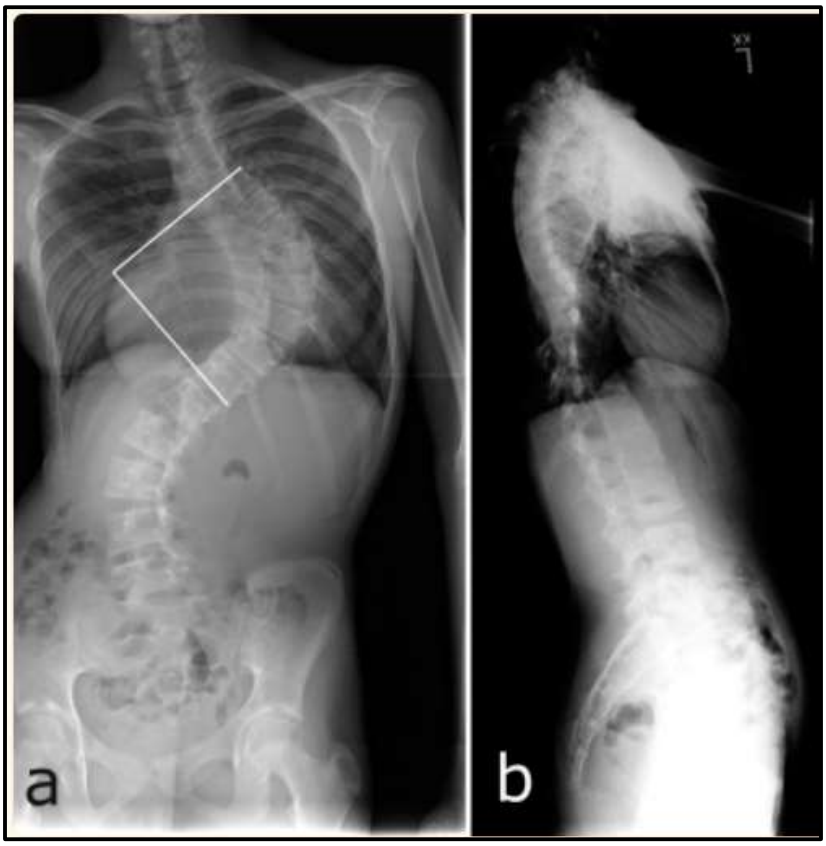

Figure 2.1: X-ray of a patient with scoliosis (7)

Typical treatment options for scoliosis include both non-operative and operative treatment options. Common non-invasive treatments include casting and bracing (2). Casting implies using traction, padding, and plaster to resist spinal rotational forces in an attempt to halt the curving of the spine. Bracing is the more common option, which simply entails using an external brace to help correct the spinal curvature using external forces (8). If caught early enough, this is all that will be required, however, 5-10% of idiopathic scoliosis cases require a surgical procedure (14). There are three main categories of surgical operations that may be used to correct the spine's unnatural curve: distraction-based, compression-based, and growth guided. These are separated by the amount of correction force applied to the spine. Distraction-based operations are the most common and include magnetically controlled growing rods (MCGRs) and vertical expandable prosthetic titanium ribs (VEPTRs). Compression-based surgeries include operations such as

vertebral body stapling (VBS) and vertebral body tethering (VBT). Examples of growth-guided surgeries include the Shilla™ system and the modern Luque™ trolley (MTR) (2).

As surgical technology advances, more surgeries of this type are being performed. According to Vigneswaran et al., from 1997 to 2012 the number of adolescent idiopathic scoliosis (AIS) surgeries increased by 193% (9). However, surgically repairing scoliosis is not easy and has a number of complications. Patient complication rates have been reported anywhere from 5.4% (11) to 22.3% (10). Examples of common complications include infection, neurological injury, or implant issues. Not only are surgical complications important to consider, but also the financial burden on families. Currently, the cost of AIS surgery ranges from $48,000 (12) to $153,000 (13), with prices tripling from the mid-90s. The steep increase in price has resulted in a market cost of over $1 billion in the United States annually (10).

2.1.1 At-Risk Populations

Scoliosis is significantly more common in children than adults and occurs in girls more often than boys (7). Scoliosis can still develop in adults but unfortunately, scoliosis is a disease that is not fully understood yet. Because of this, there is no tell-tale sign that a child will have the disease, nor is the reason the patient may have it going to be fully understood. Approximately 80% of adolescent scoliosis cases are classified as idiopathic cases, because the root of the problem is not fully understood, and the condition appears unexpectedly later in life. In the case of congenital scoliosis, which occurs when a child is born with the disease, several factors have been studied including carbon monoxide exposure, maternal diabetes, and antiepileptic medication exposure (14) but studies have not come to a concrete conclusion on the reason for the disease in newborns.

It is accepted that genetics play a role in the development of scoliosis, but only 11% of first-degree relatives are affected by scoliosis if another nuclear family member has the disease (15). Links between successive generations have not been identified, but many genes and genetic pathways have been analyzed to try to identify a possible reason. Studies have been performed using transforming growth factor-beta (TGF- β) (15), Vitamin D receptor gene (VDR) (16) and several others. One thing that has been agreed upon is that scoliosis is a multifactorial disease, simply meaning that this disease is the result of not just one but many different possible factors, genetic or otherwise.

2.1.2 Scoliosis Symptoms

Like many diseases, scoliosis can have a variety of symptoms based on the severity of the disease. In many cases, scoliosis does not directly cause pain to the patient, but patients have reported back pain to be a symptom of their disease (7). Physical discomfort is common in scoliosis cases. In severe cases pulmonary function may be affected and should be treated as soon as possible (7). More common and noticeable symptoms include uneven shoulders, hips, or chest. In adolescents particularly, this may lead to psychological issues with self-image (18) and in extreme cases lead to depression and suicidal thoughts (17).

2.1.3 Surgical Treatment Options

As the disease is better understood, treatment options continue to progress and develop. Treatment options depend on several factors including age, curve magnitude, and curve progression (19). To quantify the curve magnitude, the Cobb's angle is a standard measurement taken to assess the severity of the patient's condition, as shown in Figure 2.1. Parallel lines are drawn from the upper surface of the top vertebrae and lower surface of the lower vertebrae of the

curved region needing assessment. Perpendicular lines are created from the original lines and the angle when they intersect is the Cobb's angle (57).

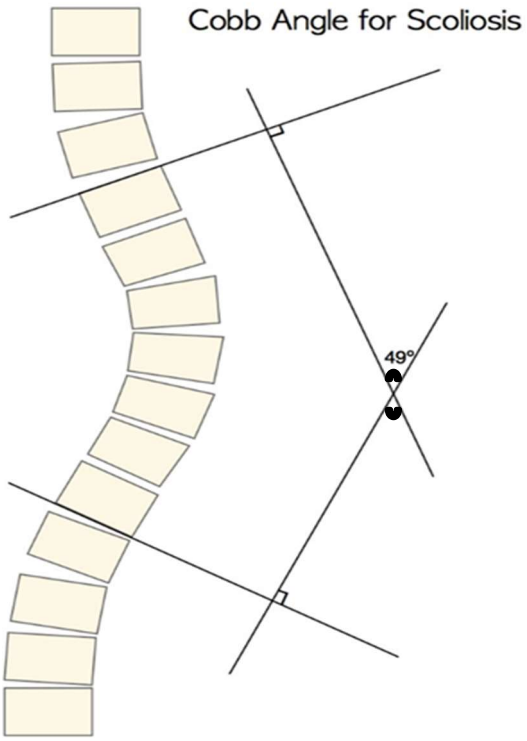

Figure 2.2: How to measure Cobb's Angle for scoliosis patients (55)

In this example, the Cobb's angle of this patient is 49 degrees. Surgical correction is considered for adolescent patients with a Cobb's angle greater than 45 degrees, and adult patients with a Cobb's angle greater than 50 degrees (20). The overall goal of surgical correction is to prevent deformity progression and correct spinal alignment. There are two main ways surgeons do this, and that is with a spinal fusion surgery (SFS) or a non-fusion surgery. SFSs will use a rigid rod to connect all the necessary vertebrae. Non-fusion surgeries are used more often in pediatric settings. This is because many children receiving surgery to treat scoliosis are still growing, so fusing the spine will shunt growth in the spine and rib cage, leading to further problems. To prevent this, growing rods are used, as they allow the child to continue growing, while also correcting the spinal deformity.

2.1.3.1 Magnetically Controlled Growing Rods

Magnetically controlled growing rods (MCGRs) are common distraction-based orthopedic implants used in pediatric spinal deformity cases, typically early onset scoliosis (EOS). For growing children, this is a preferred method of treatment because while spinal fusion surgeries stunt the growth of the spine, MCGRs assist in correcting the spine, while also allowing the spine and chest cavity to continue growing (39). Like spinal fusion rods, MCGRs are dual rod constructs with the rods being placed in pedicle screws, but only eight screws are typically inserted into the spine. The two upper vertebrae and two lower vertebrae involved in the spinal correction receive pedicle screws, and the remaining middle vertebrae are untouched. Typically, one MCGR with caudal-based distraction is applied to the left side, while the other MCGR distracts toward the cranial direction (39), allowing for separate lengthening of each rod. Rods are lengthened using an external magnetic remote controller and patients ideally return every 6 months for relengthening (40). Complications with this technique are relatively high as one study reported that 81 out of 140 (58%) of children reported at least one complication during a five-year follow-up (41).

2.1.3.2 Vertical Expandable Prosthetic Titanium Rib

The vertical expandable prosthetic titanium rib (VEPTR) system is a recently developed guided growth technique used to control scoliosis during the growth years for children with severe scoliosis. There are two constructs involved in the successful operation of the VEPTR, they can be a proximal to distal rib-to-rib device, and either a rib-to-spine device, or a rib-to-pelvis device (43). The most common complication with this method is proximal rib anchor failure (44). To use this device a thoracotomy will be performed, which displaces the ribs to expand the chest. To hold this desired position, the VEPTRs will be fused to the necessary proximal and distal points along the spine and rib cage. The patient will then return to the hospital every 6 months for the device to

be expanded to continue allowing the chest and spine to grow. Unlike the MCGR, this technique will require the patient to be opened again to expand the VEPTRs properly. Once the child has grown the device will be removed if there are no significant signs of scoliosis. If the disease persists, spinal fusion may be required.

2.1.3.3 Spinal Fusion Rods

Spinal fusion rods have been a standard of care over the last several decades. Surgical spinal fusion treatment began in the 1960s when Paul Randall Harrington created the "Harrington Rod". Before the 1990s, the idea of segmental alignment was made more realistic, and pedicle screws became an increasingly used instrument (42). Developing technology allowed clinicians to become more confident in drilling into the spine and studies soon showed the improved realignment and reliability of using pedicle screws and fusion rods. Figure 2.2 depicts how the rods and screws are positioned in the spine after a spinal fusion operation.

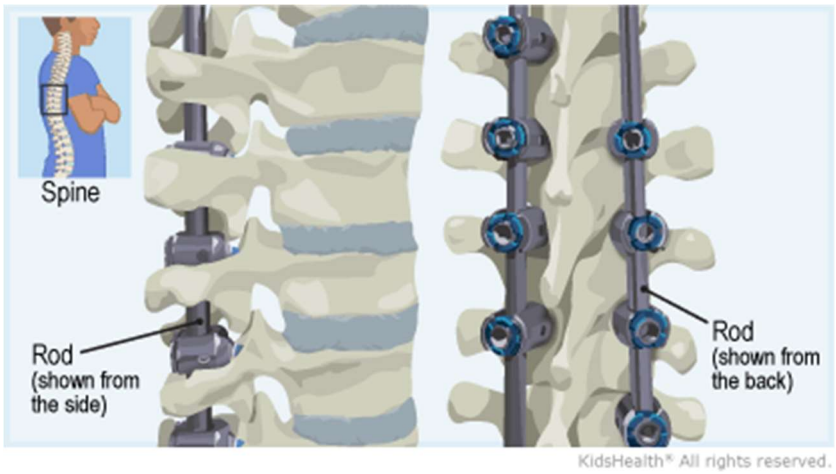

Figure 2.3: Position of rods and screws in the back after surgery (56)

Implanted spinal fusion rods, like any biomaterial, need to be both biofunctional and biocompatible. The material selected must be able to fulfill the mechanical requirements of a spinal implant. High yield strength, high fatigue strength, and stiffness are all essential factors to the material selected. Equally important, however, is the material's biocompatibility. The material

must be able to interact with the surrounding tissue and not elicit systematic responses in the body (38). Corrosion and degradation can occur at the implant site due to incompatible materials. Because of these factors, spinal fusion rods are typically made of titanium (Ti) based alloys, cobalt chrome (CoCr) based alloys, or stainless steel (SS) (37). Each material has its own desired properties and based on the surgical case the surgeon may use a different material rod. CoCr has a higher modulus of elasticity than Ti, has a high stiffness and a low yield strength and as a result, CoCr is usually implanted into the spine first, to handle the bulk of the directional correction. The Ti rod is placed in after, as it can be bent to fit the concave or convex curves still existing in the spine. CoCr rods have been reported as producing higher correction forces, but also being susceptible to experiencing more plastic deformation (49). However, metallic rods used in spinal fixation devices are required to have not only a low Young's modulus to avoid the stress shielding effect but also a high Young's modulus to suppress springback so that the implants offer better handling ability during operations (54).

2.1.4 Scoliosis Spinal Fusion Surgery

Surgeons will open the patient posteriorly and the size of the opening will be determined pre-operation based on the patient's needs. The first step is to open the patient and proceed by exposing and cleaning the spinal column. The spine needs to be cleaned well so that the pedicles and lamina can all be accessed easily by the surgeon. Once the spinal column has been cleaned the zygapophyseal joint between each vertebra is separated to see the spinal anatomy better, to free and loosen the spine in preparation for the rod implants, and the joint is needed to be removed for the screw to fit in the spine. Once this step is completed, the screws start being implanted. In neuromuscular scoliosis cases the vertebrae may be of different sizes, so different size screws are needed at different spots along the spine. Gear tools will be used to start clearing the path for the

screw to be placed. After this, a drill will be used to tap, or clear, debris in the vertebrae, and then the screw will be placed in the vertebrae.

Once all screws have been placed the rods will be inserted next. The rods come in one size, so they are first cut using a rod cutter to the desired size for the specific patient. Figure 2.4 provides an example of what standard OR rod cutters look like.

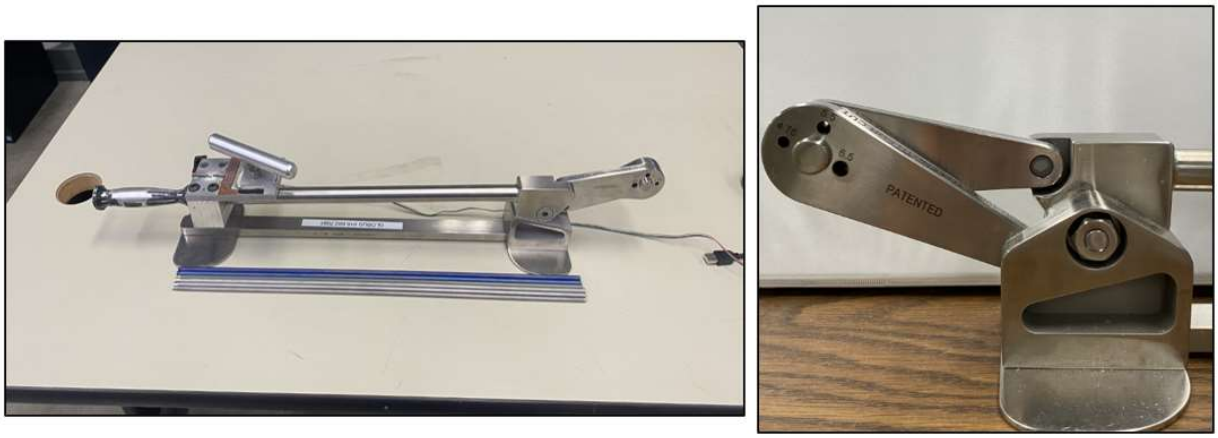

Figure 2.4: Left image is a standard OR rod cutter. Right image is zoomed in on the part which cuts the rods

Next is rod contouring where the surgeons bend the rod using French Benders to match the curves of the spine. Contouring is important to allow the rod to fit tightly along the spine and apply the proper bending forces to assist in the correction of the spine. Once the rough shape of the spine is mimicked, the rods will be sequentially placed in the screws, making sure the bottom curve of the pedicle tulip is snug with the curved rod being placed there. Surgeons will typically use one titanium (Ti) rod and one cobalt chrome (CoCr) rod when fusing. The CoCr rod is the first one to be placed. This is because CoCr is stiffer and is typically referred to as the "correction rod." Ti is more malleable and can bend more so that it will be placed in second. The rods are first implanted in the inferior screws and then placed into the following superior screws. The surgeon will then

use a tool called a sequential reductor to gradually tighten all the rods at the same time, rather than fully tighten one screw at a time. This helps with load sharing along the spine. This process is done for each rod, one after the other. Finally, bone graft is placed in and around the rods and the patient will be closed (53). Figure 2.4 provides an example of what this looks like in the body. On the left, is an x-ray of a patient's spine before their surgery. On the right, is an x-ray of the same patient after.

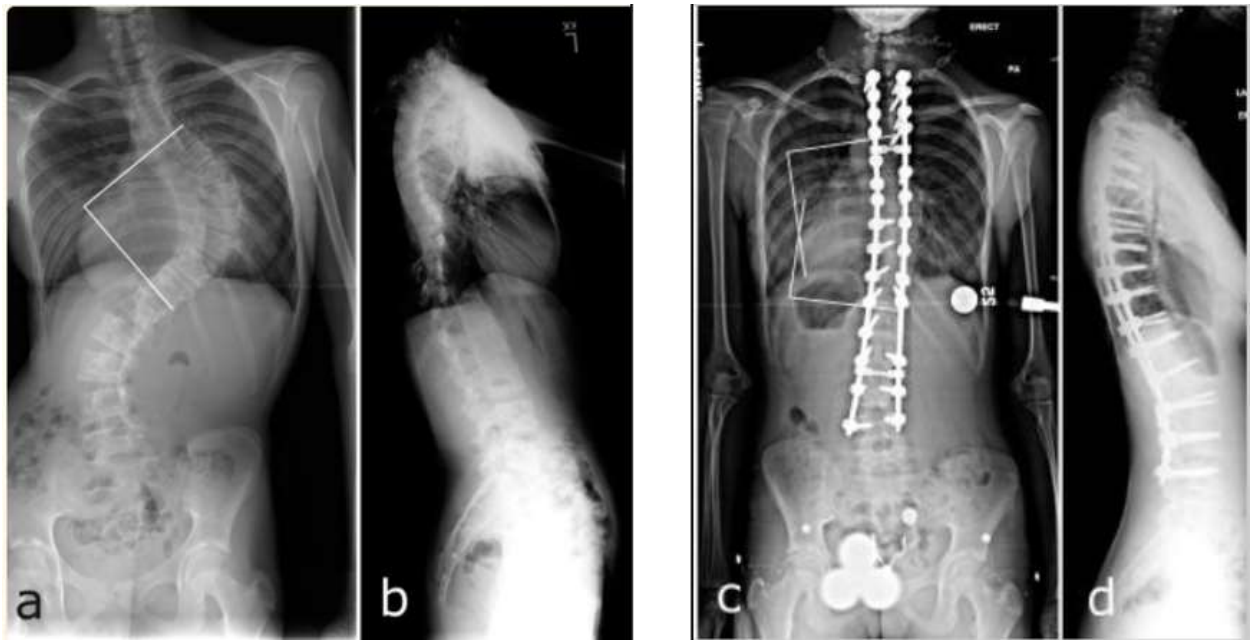

Figure 2.5: X-rays of the same patient pre and post operation (55)

2.1.5 Screw – Rod Interface

The connection between the pedicle, pedicle screw, and the spinal fusion rod is very important to the overall success of a spinal fusion correction surgery. Proper connections are extremely important, as misalignments or incorrect placements can lead to instrument failure resulting in many types of complications including death, neurological damage, loss of normal spinal function, strain on vertebrae, pain, inflammation, continued curvature progression, and

repeat surgeries (45). Figure 2.5 provides an exaggerated example of the difference between a secure connection and a deformed connection.

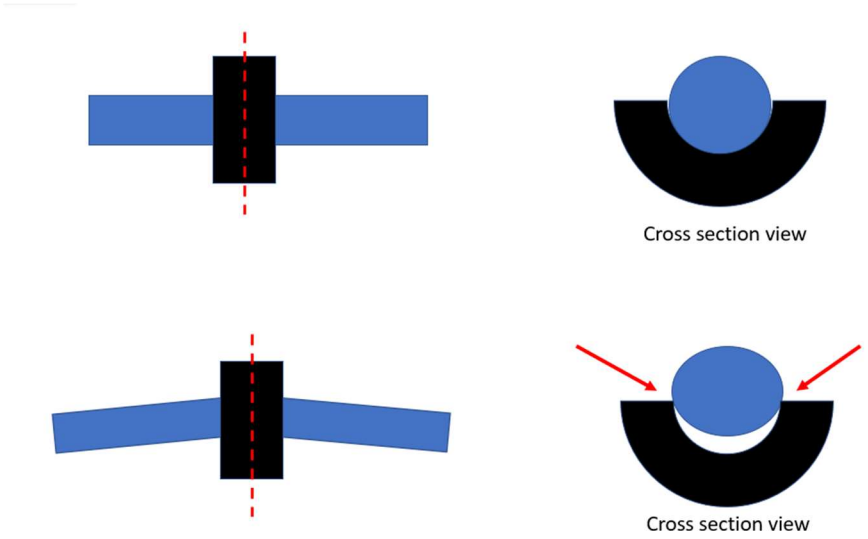

Figure 2.5: Exaggerated **s**ample view of the difference between rod sitting tightly in the pedicle screw tulip and one with deformation

Typical locations for rod failure are at the apex of a contoured rod and at the screw-rod interface (37). Reasons for instrument failure include rod deformations exceeding the tolerable limit of the pedicle screw resulting in stress concentrations, corrective forces exceeding the limit of the anchor strength of the pedicle screw, and the cyclic loading fatigue life of the rod being reached (48-50). The screws and rods undergo compressive, torsional, bending, shear, and pullout forces. Typically, these screws can withstand forces ranging from several hundred to several thousand newtons (46, 47). After the rod has been secured in the screws, the spine is not going to be perfectly straight still. There will still be an imperfect alignment of the spine, which means the corrective forces will still be at play keeping the spine in place and preventing it from reverting back to its previous state. Bending of the rod during contouring can lead to the "notch effect," which results in cracks in the rod, increasing the stress concentration and decreasing endurance of the rod (48). Rod contouring has been tested to determine the correction forces present in different

material rods, and the percentage of shape maintained after deformation via contour. When rods are bent more, higher correction forces are present in the rod (49). However, the number of loading cycles the construct can withstand decreases as contouring is introduced (50). Rod contouring is necessary to provide correction to the spine, but contours over 60 degrees at the peak of the bend result in a risk for rod fracture (51).

2.1.6 Rod Roundness

Deformation of an originally circular cross-section rod may plastically distort the cross-section so that it is no longer perfectly circular. The undeformed rod is manufactured to have a consistent diameter at any point along the length of the rod and along the perimeter of a cross section. When the rod is cut with the rod cutter, the end of the rod is subjected to high amounts of shearing force, which results in plastic deformation at the end of the rod. This deformed end still goes in the patient. It is imperative that the deformed end of the rod does not sit in the pedicle screw as that may lead to instrument failure leading to death, neurological damage, loss of normal spinal function, strain on vertebrae, pain, inflammation, continued curvature progression, and repeat surgeries (45). To avoid this, the rod should be placed in the pedicle screw only when it is known that there is no deformation in the cross section sitting in the pedicle screw tulip. Deformation can be a non-uniform circular cross section or angular deformation along the rod's edge.

ASTM F1877-16 defines roundness as a measurement of how close a particle is to a perfect circle. It has a value scale of 0-1 with a perfect circle having a roundness of 1.0 and is calculated via the following equation.

$$\frac{4A}{\pi \cdot (Major\ Axis^2)}$$

This equation can be used to measure the cross sections of a deformed rod and determine how close to a perfect circle the cross section is. It can be used to determine how much deformation occurs at the end of each rod and at what point the rod no longer experiences any circular deformation from the rod cutter.

2.2 Photogrammetry

Photogrammetry is a technique used to ascertain three-dimensional digital models via a series of two-dimensional photographs (21). It is garnering popularity as the method creates quality models while being cheap and accessible. Photogrammetry is especially helpful in situations where an object's dimensions may be difficult to measure, there are deformations, or where topographic or contour data is necessary (29). There are two broad categories that photogrammetry sections off into, those being aerial and terrestrial photogrammetry. Aerial photogrammetry involves taking photographs from the sky to acquire data about the topography of the photographed area (22). Aerial photogrammetry is a powerful tool for archeological studies or environmental studies such as glacial geomorphology (23). Terrestrial photogrammetry does the same thing, but instead of taking pictures from the sky, the camera and photographed objects are both on the Earth's surface. When the distance from the camera to the object is less than 100m, terrestrial photogrammetry may be identified as close-range photogrammetry (21).

2.2.1 Close Range Photography

Close-range photogrammetry (CRP) is said to have been invented back in the 1840s by a Frenchman named Aimé Laussedat. Laussedat used what is now called "close-range photogrammetry" to create a map of Paris using pictures from rooftops (21). Today, his technique has been applied in a wide range of industry fields, including architecture (24), aerospace (25),

and biology (26), and has been used for an even wider range of projects. As camera and computer technology have advanced, the accessibility of CRP has been made more and more feasible, and projects may be much more complex than even 20 years ago. In addition to more complex models, more precise measurements may be made as well. With one camera, measurements as precise as 5 μm can be made (27). Using similar points in different images, photogrammetry software takes geometric data from the photographs and can create extremely accurate 3D models. To do this, triangulation is used to calculate the 3D coordinates from the 2D images. The core tenant of all photogrammetry projects remains the same no matter the field or project. To acquire the final model, numerous photographs of the desired object/area must be taken from many angles. The way this is done will change based on the project and photogrammetry type, but adequate image samples are necessary in all projects.

2.2.2 Photogrammetry Software and Algorithm

Because of the ease of use and feasible accessibility, many companies have created their own photogrammetry software. Commercial licenses include Photomodeler, Autodesk ReCap, RealityCapture, and 3DF Zephyr. Considering this, open-source software has also been developed for recreational users. Open-source software such as Meshroom, Regard3D, and VisualSFM are all free photogrammetry software (29).

Photogrammetry is based on the idea of using overlapping images to create a 3D model. To achieve this, the computer will analyze the photographs provided and start finding common points among the images, the beginning of the triangulation process. Advanced software, like the ones mentioned above, use a process called bundle triangulation. This occurs when coordinates are calculated across many photographs. After doing this repeatedly, the program will generate a sparse point cloud. The sparse point cloud is a quick and simple rendering of the basic geometry

of the photographed object (28). Once the sparse point cloud is created, the program will begin building more points into the point cloud until all features and geometries are represented. A process known as “surface triangulation” will then be employed to generate the triangulated mesh. Finally, the mesh will be textured using data from the supplied images to create the final product. Photogrammetry software is not able to calculate real distances, so local coordinate systems are created in the building of the model, and then the user can scale the model down or up to its actual size.

2.2.3 Applications of Photogrammetry

Photogrammetry is used in a wide range of industry fields and with advanced camera and computer technology, is becoming increasingly popular with a wider range of applications. A society-wide wave of combining the physical with the digital is improving processes in every industry field.

2.2.3.1 Dental Applications

Patient dental models are an important part of the practice that assists dentists in preparing for surgery, implant planning, and restoration treatment. In a standard treatment, computed tomography (CT) scans are used to reproduce a digital scan of the mouth. To reduce the need for exposing patients to radiation, accurate 3D scanners that did not use radiation started hitting the dental market. However, the high price tag of these scanners turned some professionals away and they looked for other options. For this reason, photogrammetry was utilized in the dental sector due to its low cost, yet relatively high accuracy and availability. In a study conducted at the University of Sao Paulo, Stuani et al acquired a plaster model of a mouth and used photogrammetry to create 5 digital models of the plaster model (34). Digital models were made using 50 images. Measurements of each model were then made and later statistically compared to the original,

physical model. Discrepancies across the digital models ranged from –0.5mm to +0.5mm off the original model. Using open-source software, this team was able to replicate the human mouth model with acceptable accuracy at little to no cost.

2.2.3.2 Biology Applications

In the biology field, morphology studies are very common. Morphology is the study of the size and shape of things. Photogrammetry is a powerful tool for measuring the size and shape of difficult-to-measure objects. The ability to use photogrammetry to represent what was once represented by 2D data has proven very useful for biologists measuring these things. One example of this is using photogrammetry to measure morphological traits in deer antlers (30). Cervid antlers are commonly analyzed to determine orthogenesis, heterochrony, allometry, and even stress levels in deer populations based on the volume of the antlers. A team from Norway decided to use photogrammetry to analyze their cervid antlers instead of 2D data. Using photogrammetry, they constructed detailed models of deer antlers and measured both length and volume. They compared the model's measurements to antlers with known length and volume to test accuracy and bias and deemed that photogrammetry was an acceptable method of measuring the phenotypic features of deer antlers. In their study, AutoDesk ReCap Photo 2017 was the program of choice. Approximately 50 pictures were used to make each model resulting in a relative error of 8.5%. In addition to deer antlers, photogrammetry morphology studies have been performed on bat skulls (26), coral reef habitats (31), and bottlenose dolphin populations (32).

2.2.3.3 Aerospace Applications

To be successful, aircraft components must be manufactured to an extremely precise level. Small defects on parts that are subject to extreme conditions can have catastrophic consequences. In the aerospace industry, small defects are common and can occur from sources such as bird

strikes, weather damage, and improper maintenance. Because of this, maintenance inspections are routinely carried out to ensure every aircraft is at no risk of further damage. However, there is a certain difficulty that comes with measuring large parts of the aircraft, such as the fuselage or the empennage. To combat this, industry workers have used photogrammetry with an unmanned aerial vehicle (UAV) to create models of these parts, allowing maintenance teams to measure the 3D models of the aircraft, rather than the aircraft itself (33). Aldao et al used this strategy to measure a dented aluminum plate and airplane propeller. The purpose of their study was to compare the results of three different modes of photogrammetry, those being an Xbox One Kinect sensor, a stereo camera ZED, and the Sony Alpha 6000, a digital camera. Three different objects were modeled using the three different modes. When modeling the propeller, the digital camera resulted in the smallest amount of error, around 1.25%. The propeller was 1.35m wide and was accurate to approximately 20mm. This shows that photogrammetry has the potential to create very accurate models for difficult to measure objects, both large and small.

Chapter 2 References

1. Janicki, J.A., MD, Alman, B., MD, *Scoliosis: Review of Diagnosis and Treatment*. Paediatrics & Child Health. 2007. **12**(9): p.771–776.
2. Zhang Y.B., Zhang J.G., *Treatment of Early-Onset Scoliosis: Techniques, Indications, and Complications*. Chin Med J (Engl). 2020. **133**(3): p. 351-357.
3. Hardesty C.K., et al., *Early-Onset Scoliosis: Updated Treatment Techniques and Results*, Spine Deform. 2018. **6**(4): p. 467-472.
4. Shakil H., Iqbal Z.A., Al-Ghadir A.H., *Scoliosis: Review of Types of Curves, Etiological Theories and Conservative Treatment*. J Back Musculoskelet Rehabil. 2014. **27**(2): p.111-115.
5. Kouwenhoven, J. M. & Castelein, R. M., *The Pathogenesis of Adolescent Idiopathic Scoliosis*. Spine. 2008. **33**(26): p. 2898-2908.
6. Yaman O., Dalbayrak S., *Idiopathic scoliosis*. Turk Neurosurg. 2014. **24**(5): p. 646-657.
7. Trobisch P, Suess O, Schwab F. *Idiopathic scoliosis*. Dtsch Arztebl Int. 2010. **107**(49): p. 875-883.
8. Weinstein S.L., Dolan L.A., Wright J.G., Dobbs M.B., *Effects of Bracing in Adolescents with Idiopathic Scoliosis*. N Engl J Med. 2013. **369**(16): p. 1512-1521.
9. Omar A., et al., *Surgical treatment of adolescent idiopathic scoliosis: Complications*, Annals of Medicine and Surgery. 2020, **52**: p. 19-23.
10. Vigneswaran, H. T., Grabel, Z. J., Eberson, C. P., Palumbo, M. A., & Daniels, A. H., *Surgical Treatment of Adolescent Idiopathic Scoliosis in The United States From 1997 To 2012: An Analysis Of 20,346 Patients*. Journal of Neurosurgery: Pediatrics PED. 2015. **16**(3): p. 322-328.
11. Bartley, Carrie E., et al., *Perioperative and Delayed Major Complications Following Surgical Treatment of Adolescent Idiopathic Scoliosis*. The Journal of Bone and Joint Surgery. 2017. **99**(14): p. 1206-1212.
12. Baky, F.J., Echternacht, S.R., Milbrandt, T.A., et al., *Predictors of Cost For Posterior Spinal Fusion In Adolescent Idiopathic Scoliosis*. Spine Deform. 2020. **8**: p. 421–426.
13. Daffner, S.D., Beimesch, C.F., Wang, J.C., *Geographic and Demographic Variability of Cost and Surgical Treatment of Idiopathic Scoliosis*. Spine. 2010. **35**(11): p. 1165-1169.
14. Heary, R.F., Madhavan, K., *Genetics of Scoliosis*. Neurosurgery. 2008. **63**(3): p. A222-A227.
15. Nowak R., Kwiecien M., Tkacz M., Mazurek U., *Transforming Growth Factor-Beta (TGF- B) Signaling in Paravertebral Muscles in Juvenile and Adolescent Idiopathic Scoliosis*. Biomed Res Int. 2014. **2014**: 594287.
16. Nowak R., Szota J., Mazurek U., *Vitamin D Receptor Gene (VDR) Transcripts In Bone, Cartilage, Muscles And Blood And Microarray Analysis Of Vitamin D Responsive Genes Expression In Paravertebral Muscles Of Juvenile And Adolescent Idiopathic Scoliosis Patients*. BMC Musculoskelet Disord. 2012. **13**: p.259.
17. Payne W.K., Ogilvie J.W., Resnick M.D., Kane R.L., Transfeldt E.E., Blum R.W., *Does Scoliosis Have a Psychological Impact and Does Gender Make a Difference?* Spine. 1997. **22**(12): p. 1380 – 1384.
18. Freidel K., Petermann F., Reichel D., Steiner A., Warschburger P., Weiss H.R., *Quality of Life In Women With Idiopathic Scoliosis*. Spine. 2002. **27**(4): p. E87 – E91.

19. Janicki, J.A., MD, Alman, B., MD, *Scoliosis: Review of Diagnosis and Treatment*. Paediatrics & Child Health. 2007. **12**(9): p. 771–776.
20. Lovell W.W., Winter R.B., *Lovell and Winter's 'Pediatric Orthopaedics' 5th ed., Vol. II*. Philadelphia: Lippincott William & Wilkins; 2001.
21. Jiang, R., Jáuregui, D.V., White, K.R., *Close-Range Photogrammetry Applications in Bridge Measurement: Literature Review*. Measurement. 2008. **41**(8): p. 823-834.
22. Nikolakopoulos, K.G., et al., *UAV vs Classical Aerial Photogrammetry for Archaeological Studies*. Journal of Archaeological Science: Reports. 2017. **14**: p. 758-773.
23. Śledź, S., Ewertowski, M.W., Piekarczyk, J., *Applications of Unmanned Aerial Vehicle (UAV) Surveys and Structure from Motion Photogrammetry in Glacial and Periglacial Geomorphology*. Geomorphology. 2021. **378**: 107620.
24. Yilmaz, H.M., Yakar, M., Gulec, S.A., Dulgerler, O.N., *Importance of Digital Close-Range Photogrammetry in Documentation of Cultural Heritage*. Journal of Cultural Heritage. 2007. **8**(4): p. 428-433.
25. Liu, T., et al*., Photogrammetric Techniques for Aerospace Applications*. Progress in Aerospace Sciences. 2012. **54**: p. 1-58.
26. Giacomini, G., Scaravelli, D., Herrel, A., et al., *3D Photogrammetry of Bat Skulls: Perspectives for Macro-Evolutionary Analyses*. Evol Biol. 2019. **46**; p. 249–259
27. Jing, X., Zhang, C., Sun, Z., Zhao, G., Wang, Y., *The Technologies of Close-range Photogrammetry and Application in Manufacture*. International Congress of Mathematicians. 2015.
28. Duong, N.N., *A Comparative Case Study Between Agisoft Photoscan and Autodesk Recap Photo-To-3D Web Services*. 2018. Tampere University of Applied Sciences. Master's Thesis.
29. Potabatti, N.S., *Photogrammetry For 3D Reconstruction In Solidworks And Its Applications In Industry*. 2019. Purdue University Graduate School. Master's Thesis.
30. Tsuboi, M., Kopperud, B.T., Syrowatka, C., et al., *Measuring Complex Morphological Traits with 3D Photogrammetry: A Case Study with Deer Antlers*. Evol Biol. 2020. **47**. p. 175–186.
31. Anelli, M., et al., *Towards New Applications of Underwater Photogrammetry for Investigating Coral Reef Morphology and Habitat Complexity in The Myeik Archipelago, Myanmar*. Geocarto International. 2019. **34**(5): p. 459-472.
32. van Aswegen, M., Christiansen, F., Symons, J., et al., *Morphological Differences Between Coastal Bottlenose Dolphin (Tursiops Aduncus) Populations Identified Using Non-Invasive Stereo-Laser Photogrammetry*. Sci Rep**.** 2019. **9**: n. pag.
33. Aldao, E., González-Jorge, H., Pérez, J.A., *Metrological Comparison of Lidar and Photogrammetric Systems for Deformation Monitoring of Aerospace Parts*. Measurement. 2021. **174**: 109037.
34. Stuani, V.T., *Photogrammetry as An Alternative for Acquiring Digital Dental Models: A Proof of Concept*. Medical Hypotheses. Volume 128. 2019. p. 43-49.
35. Allam, A.M., Schwabe, A.L., *Neuromuscular Scoliosis*. PM&R. 2013. **5**(11): p. 957-963.
36. Hedequist, D., Emans, J., *Congenital Scoliosis: A Review and Update*. Journal of Pediatric Orthopaedics. 2007. **27**(1): p 106-116.
37. Yoshihara, H. *Rods in Spinal Surgery: A Review Of The Literature*. The Spine Journal.. 2013. **13**(10): p. 1350-1358.

38. Lane, J.M., et al., *Materials in Fracture Fixation*. Comprehensive Biomaterials. 2011. **6**: p. 219-235.
39. Helenius, I.J., *Standard and Magnetically Controlled Growing Rods for The Treatment Of Early Onset Scoliosis*. Ann Transl Med. 2020. **8**(2): p. 26.
40. Hosseini, P., et al., *Magnetically Controlled Growing Rods for Early-Onset Scoliosis: A Multicenter Study Of 23 Cases with Minimum 2 Years Follow-Up*. Spine. 2016. **41**(18): p 1456-1462.
41. Bess, S., et al., *Complications of Growing-Rod Treatment for Early-Onset Scoliosis: Analysis of One Hundred and Forty Patients*. The Journal of Bone & Joint Surgery. 2010. **92**(15): p 2533-2543.
42. Gautschi, O. P., Schatlo, B., Schaller, K., & Tessitore, E., *Clinically Relevant Complications Related to Pedicle Screw Placement in Thoracolumbar Surgery and Their Management: A Literature Review Of 35,630 Pedicle Screws*. Neurosurgical Focus. 2010. **31**(4): p. E8.
43. Parnell, S.E., Effmann, E.L., Song, K., et al., *Vertical Expandable Prosthetic Titanium Rib (VEPTR): A Review of Indications, Normal Radiographic Appearance and Complications*. Pediatr Radiol. 2015. **45**: p. 606–616.
44. Campbell, R.M., et al., *The Effect of Mid-Thoracic VEPTR Opening Wedge Thoracostomy on Cervical Tilt Associated With Congenital Thoracic Scoliosis in Patients With Thoracic Insufficiency Syndrome*. Spine. 2007. **32**(20): p. 2171-2177.
45. Weiss, H.R., Goodall, D., *Rate of Complications in Scoliosis Surgery – A Systematic Review Of The Pub Med Literature*. Scoliosis. 2008. **3**: p. 9-9.
46. Abe, Y., Ito, M., Abumi, K., et al., *Scoliosis corrective force estimation from the implanted rod deformation using 3D-FEM analysis*. Scoliosis. 2015. **10**. S2.
47. Pfeiffer, M., et al., *Effect of Specimen Fixation Method on Pullout Tests of Pedicle Screws*. Spine. 1996. **21**(9): p. 1037-1044.
48. Ohrt-Nissen S., Dahl B., Gehrchen M., *Choice of Rods in Surgical Treatment of Adolescent Idiopathic Scoliosis: What Are the Clinical Implications of Biomechanical Properties? - A Review of the Literature*. Neurospine. 2018. **15**(2): p. 123-130.
49. Serhan, H., et al., *Would CoCr Rods Provide Better Correctional Forces Than Stainless Steel or Titanium for Rigid Scoliosis Curves?*. Journal of Spinal Disorders and Techniques. 2013. **26**(2): p. E70-E74.
50. Piovesan, A., Berti, F., Villa, T., Pennati, G., La Barbera, L., *Computational and Experimental Fatigue Analysis of Contoured Spinal Rods*. J Biomech Eng. 2019; **141**(4). n. pag.
51. Barton, C., Noshchenko, A., Patel, V., et al., *Risk Factors for Rod Fracture After Posterior Correction of Adult Spinal Deformity with Osteotomy: A Retrospective Case-Series*. Scoliosis. 2015. **10**: p. 30.
52. Warburton A., Girdler S.J., Mikhail C.M., Ahn A., Cho S.K., *Biomaterials in Spinal Implants: A Review*. Neurospine. 2020. **17**(1): p. 101-110.
53. Frederick, A., James, M., Beaty, H., Canale, S.T., Campbell, W.C., *Campbell's Operative Orthopaedics (version 14th edition).* 14th ed. Philadelphia PA: Elsevier. 2021.
54. Nakai, M., et al., *Self-Adjustment of Young's Modulus in Biomedical Titanium Alloys During Orthopaedic Operation*. Materials Letters. 2011. **65**(4). p. 688-690.
55. "Spinal Fusion Surgery (for Parents) - Nemours Kidshealth." Edited by Suken A. Shah, *KidsHealth*, Jan. 2022, kidshealth.org/en/parents/spinal-fusion.html.

56. Texas, LF •, et al. “Cobb Angle Measurement.” *Scoliosis 3DC®*, scoliosis3dc.com/scoliosis-resources/cobb-angle-measurement/.
57. James, J. (1976) Scoliosis, Churchill Livingstone, London, pg 7-11 1A

Chapter 3: Analysis of Scoliosis Rod Deformation After Cutting with a Surgical Rod Cutter

This section contains a manuscript to be submitted for publication, some information is duplicated
Target Journal: Journal of Bone and Joint Surgery

Abstract

Background:

Scoliosis leads to spine deformity with lateral curvature, common in children and adults. Treatment using spinal fusion rods typically use titanium, cobalt-chrome, and stainless steel. Rods are cut during surgery, raising concerns about deformation at the cut end. This study examines rod deformation from the rod cutter and optimal placement from pedicle screws. Insights aid clinical decisions, guiding placement and minimizing deformation in pedicle screw tulip. Such understanding reduces risk of construct failure, spinal complications, and informs surgical planning for effective correction.

Methods:

This study was performed using photogrammetry, a technique allowing the creation of 3D models from photographs. Rod metals included titanium (Ti) and cobalt chrome (CoCr). Three different diameters, 4.75 mm, 5.5 mm, and 6.0 mm were analyzed for each metal. Deformed rods were photographed, modeled, and measured. The parameters measured include local angle of deformation at each mm away from the cut, as well as roundness of the cross section. Means and standard deviations were taken for each measurement.

Results:

5 rods in each rod group resulted in the analysis of 30 total spinal fusion rods. Deformation from the rod cutter resulted in more angular deformation in the CoCr rods than the Ti rods. The CoCr rods also had lower cross sectional roundness measurements. The 6.0 mm rods had significantly more angular deformation as well as lower roundness measurements compared to the smaller diameter rods. The 4.75 mm and 5.5 mm diameter Ti rods experience 4 mm of deformation, while the 6.0 Ti rods, and all the CoCr rods experience 5 mm of deformation.

Conclusions:

It is crucial to leave the required room to decrease the chances of instrument failure. Deformation of the rod while sitting in the pedicle screw increases this chance. Typical locations for instrument failure are at the apex of a contour, or the screw-rod interface. Thus, leaving the proper amount of space between the deformed end to an area of minimal deformation is very important to reduce repeat surgeries.

Introduction

Scoliosis is a common deformity of the spine which predominantly produces lateral curvature of the vertebral column and can subsequently develop multiplanar deformity (1,2). This deformity is most identified in the pediatric population; however, can be found in the adult population as well. Several methods of deformity correction are commonly used, with both operative and nonoperative treatments (3). Some of the common operative techniques includes magnetically controlled growing rods (MCGR), vertical expandable prosthetic titanium rib system

(VEPTR), the Shilla growth guidance system, as well as anterior and posterior spinal fusion rods (3, 4, 5). The metals which are most commonly used for rod composition are generally titanium (Ti) alloys, cobalt-chrome (CoCr) alloys, or even stainless steel (SS) due to widely-accepted biocompatibility, especially for Ti and CoCr, as well as varying mechanical properties of these materials (6, 7).

With the increasing use of rods as instrumentation for deformity correction and fusion, questions have been raised regarding how mechanical properties of the rods influence mechanical deformation behavior when being handled intraoperatively. During surgery, most rods are sectioned with a rod cutter to tailor it to the correct length of deformity which needs to be corrected prior to being further contoured for final correctional positioning. Though there has been prior work analyzing deformation of instrumentation during final positioning of implants (8), there appears to be a paucity of data regarding the amount of deformation the cut end of the rod experiences. Clinically this poses a problem, as the rods are designed to fit evenly within the concavity of the pedicle screw tulip, thus potentially predisposing the surgical construct to failure due to a mismatch between rod and tulip (9). Failure of instrumentation and concomitantly fusion poses a greater risk to the progression of spinal curvature, leading to further sequalae such as the need for salvage procedures, continued pain, as well as possible neurological complications (10).

The purpose of this study was to evaluate the deformation of the cut ends of the spinal rods, as well as to determine optimal distance of placement of the end of the rod from the pedicle screw. Characterizing rod deformation will aid in guiding clinical practice for optimizing the rod-pedicle screw interface by determining the area along the length of the rod where minimal deformation occurs. Knowing where minimal deformation occurs will help inform surgeons to plan for extra rod length to eliminate the more deformed end being placed in the tulip of the pedicle screw. The

hypothesis of this study was that rods with a higher elastic modulus, being the cobalt-chrome rods in the present study, would exhibit less deformation than rods of lower elastic modulus (titanium rods). It was also hypothesized that increasing rod diameter would exhibit less deformation.

Methods

Camera Setup

To capture the required images for model generation, the Minolta MN35Z camera was used. With the ability to capture 20MP photos, the resolution was sufficient as most cameras above 16MP have similar results in photogrammetric models (11). This camera was also chosen because it has the ability to connect to a phone via Bluetooth and remotely take pictures. Having remote function was important in order to ensure the camera remained completely untouched during the photography session, to eliminate camera repositing issues. The camera was placed on a stand 9 mm away from the rod being photographed. A white, neutral background was placed behind the object. Overhead lights were left on, and two lamps with the same lightbulb were also placed on either side of the camera to apply uniform and diffuse light. A simplified version of the setup is shown in Figure 3.1.

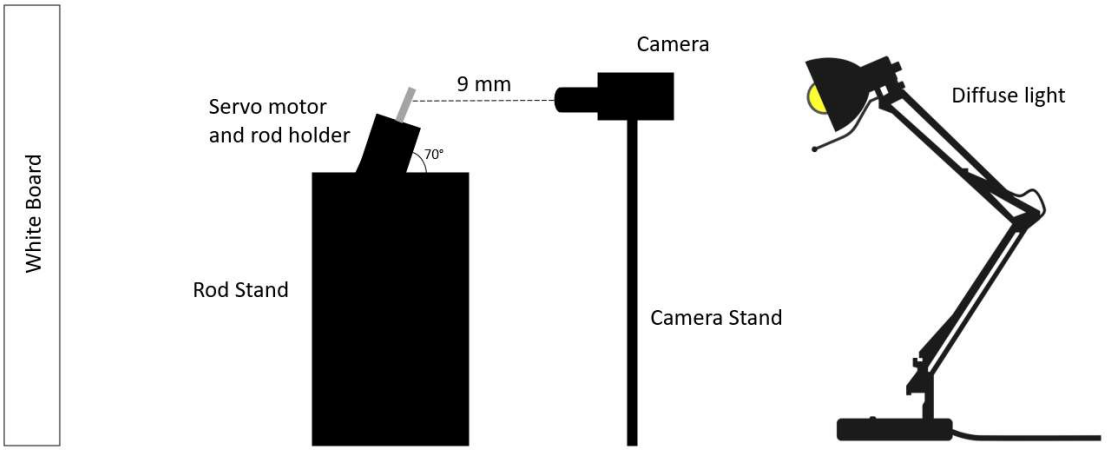

Figure 3.1: Camera setup during the photography session

Particle Preparation

Medtronic spinal fusion rods of two different materials, Ti and CoCr, and three different diameters, 4.75 mm, 5.5 mm, 6.0 mm have been selected to analyze the deformation at the end after cutting the rod with a Globus Medical tabletop rod cutter. These types of metal and diameter size are commonly used in the operating room today. The six groups each contained 5 rods of 500mm, resulting in 30 total specimens. The 500mm rod was cut at the 375mm mark. The end of the 375mm section of rod was the end of interest as it provides an approximation as to how much rod length is used in surgery. To isolate this area, a diamond saw was used to cut the rod 2 cm from the edge of the cut. This 2 cm section of rod is the part of the rod that was photographed and modeled. For the control rods, the 2 cm section was cut on both ends with the diamond saw to simulate no deformation. With such a small object, it was found to be more efficient to rotate the object of interest and keep the camera still, rather than have the camera move around the object. Marks were made on the object with ink to assist the photogrammetry software. With a homogenous object such as a cylinder of constant color, markings are necessary to provide the computer program with some sort of pattern. Additionally, three rod holders were 3d printed, one for each diameter tested. Once the rods were placed in their respective holders, they were hot glued to a servo motor plate with multicolored tape (as an additional pattern) and this construct was attached to a servo motor. The servo motor was held at a 70-degree angle to assist in depth for the photogrammetry software. Figure 3.2 details a workflow of the steps required once the rods have all been prepared.

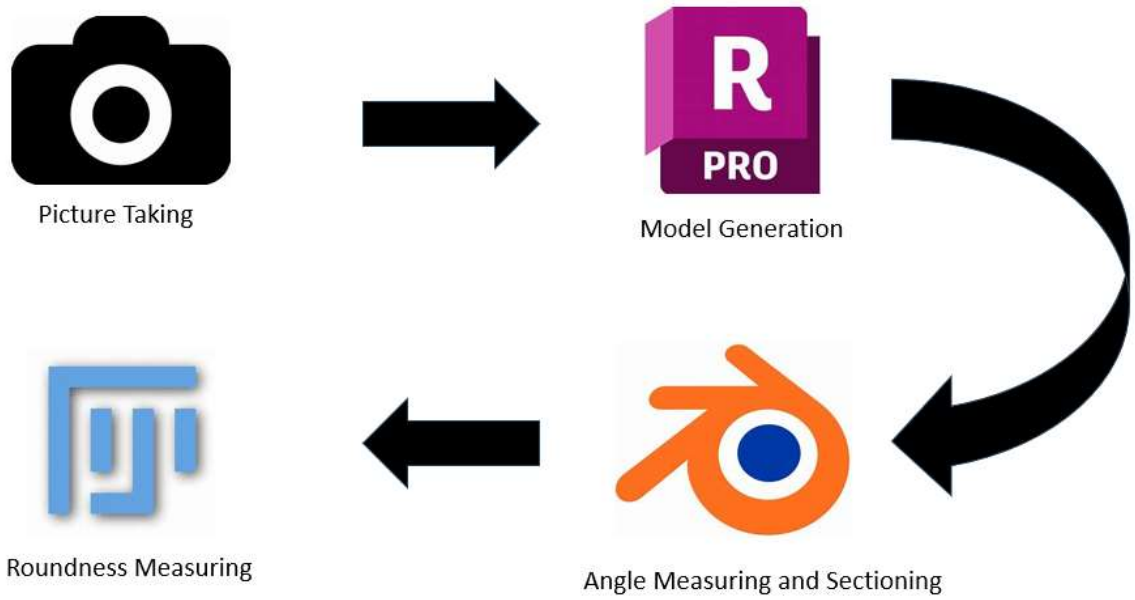

Figure 3.2: Workflow categorizing the major sections of photogrammetry steps

Photography Session

The servo motor was programmed to rotate 3.6 degrees so that 100 pictures with 20MP of resolution would be taken for a complete revolution. After rotating 3.6 degrees, the servo would stop for 4 seconds to allow for the image to be captured. This process was repeated until all 100 images were taken. An exposure value of 0.3EV was selected to increase the brightness slightly, and the TF2 whiteness filter was selected to keep the image filter constant. All other settings such as aperture, exposure time, and ISO values were all kept on automatic.

Model Generation

The images were uploaded to AutoDesk ReCap 2022 Student Version. This software was chosen over other open-source software based on the quality of the models generated using the same images. VisualSFM and ReCap are two commonly used open-source photogrammetry

software in literature. Several models using the same set of images were rendered and measured. ReCap provided more accurate measurements than VisualSFM. Creating the ReCap model may take anywhere from 1-24 hours with the student version. Once the ReCap model is generated, as shown in Figure 3.2, it is exported as an obj file to Blender 3.4.

Figure 3.3: 3D model in AutoDesk ReCap Photo 2022 with ink markings and multicolored tape

Measurements

The file was opened in Blender and measurements were taken. First, the proper scale of the model was set. The software estimates the size of the object but requires some manual measurement for more accurate estimation. The real rod was measured at the bottom of the rod with a set of calipers. The same location was then measured on the 3D model using the measure tool. The scale factor was set as the actual rod measurement divided by the raw photogrammetry measurement. Once the scale factor was determined, the model was rotated about the y-axis so

that the left side of the model represents the maximum amount of angular deformation experienced, as shown in Figure 3.3.

Figure 3.4: Zero degree location for this rod showing maximum deformation

Once the model was aligned, that view was determined as the “0 degree” view. A tangent line was made at every mm from 1 to 5 mm. The model was then sectioned along these lines using the bisect tool, and angle measurements were taken between each mm mark. For example, Figure 3.4 shows the angle measured between two different mm marks. The rod was then rotated 45 degrees and the same angle measurements were taken. Finally, the rod was rotated 90 degrees from the initial position and angle measurements were taken again.

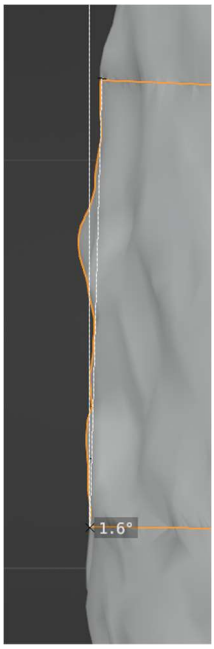

Figure 3.5: A close up view of an edge of a Blender photogrammetry model depicting how local angle changes were measured

The last set of measurements taken was roundness measurements. For this, the model was viewed from the top. The model was darkened using the viewport shading option so there is contrast between the model and the background grid. The top bisected segment was hidden, and the circular cross section is viewed, as seen in Figure 3.5. Figure 3.5 shows the comparison between an undeformed cross section and a deformed cross section.

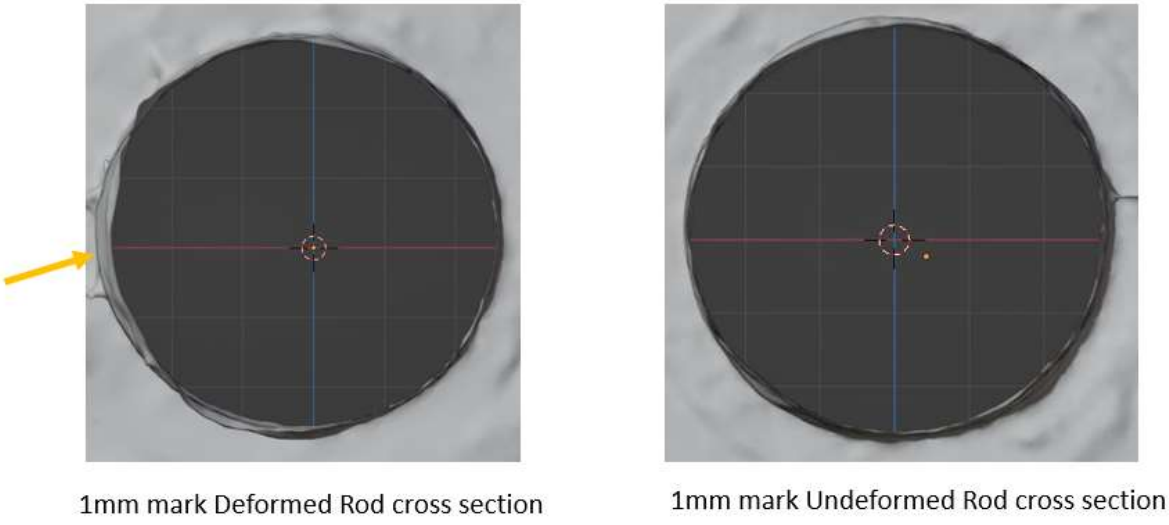

Figure 3.6: Comparison between a deformed and undeformed cross section of the rod

A screen capture was taken using Greenshot to take a picture of the circular cross section. This process was repeated for each mm along a rod. The images were then uploaded to ImageJ and roundness values were taken. The distance between the end of the rod to minimal deformation is where there appears to be no statistical significance in any deformation values between segments along the cut end of the rod.

Statistical Methods

Statistical analysis was performed on angle and roundness measurements and completed by including descriptive (mean and SD) analysis, a two-way analysis of variance (ANOVA), and a Tukey post-hoc test for comparisons of the significantly different groups. ANOVAs were performed in R Studio between the two independent variables: the metal type and the rod diameter. This is to determine if there was statistically different data between the different metal types and different rod diameters. To determine which groups specifically were different, the Tukey post-hoc test was performed in R Studio as well. Statistical significance was indicated at $p<0.05$.

Results

Angle of Deformation

Deformation in the rod caused by the shearing forces from the rod cutter resulted in bending of the end of the rod. Table 3.1 represents the angle from vertical of the instantaneous slope of the line at the 1 mm mark, 2 mm mark, and so on. The 0° and 90° viewing locations are presented.

For zero-degree angular measurements at 1 mm, there were significant differences between Ti and CoCr in the 5.5 and 6.0 groups ($p = 0.0001$ and $p = 0.0001$ respectively). There were also significant differences between CoCr rods of 4.75 mm and 5.5 mm ($p = 0.0001$), as well as 4.75 mm and 6.0 mm ($p = 0.0001$) at 1 mm. For Ti rods, the 4.75 and 6.0 groups had a statistical difference ($p = 0.0411$) as well as the 5.5 and 6.0 groups ($p = 0.0332$). At 2 mm there was no statistical significance among any group. At 3 mm, there was no statistical difference between metals based on diameter. However, based on metals there were significant differences between diameters. For CoCr, there is a significant difference between 4.75 mm and 6.0 mm ($p = 0.01$) and 5.5 mm and 6.0 mm ($p = 0.003$). For the Ti rods, there was a significant difference between the same groups with $p = 0.01$ and $p = 0.03$, respectively. At 4mm, similar to the 2 mm mark, there was no statistical difference between metals based on diameter. However, based on metals there were significant differences between diameters. For CoCr, there was a significant difference between 4.75 and 6.0 ($p = 0.047$), and for Ti there is a significant difference between 4.75 and 6.0 ($p = 0.02$) and 5.5 and 6.0 ($p = 0.02$). At 5 mm there was no longer any angular deformations observed.

Table 3.1: Deformation Angle Following Rod Cutting

Distance from cut end (mm)	Position (degrees)	4.75 Ti	4.75 CoCr	5.5 Ti	5.5 CoCr	6.0 Ti	6.0 CoCr
1	0°	1.70° ± 1.24	2.20° ± 0.68	1.55° ± 0.91	-5.75° ± 2.46	5.60° ± 2.81	-7.95° ± 1.24
	90°	1.05° ± 1.82	0 ± 0	3.05° ± 3.15	0.65° ± 0.68	0 ± 0	0.70° ± 1.21
2	0°	4.10° ± 1.24	3.00° ± 1.20	2.07° ± 0.65	2.25° ± 1.51	4.90° ± 2.2	2.58° ± 2.4
	90°	0 ± 0	0.63° ± 1.08	0.65° ± 1.13	0 ± 0	0 ± 0	4.38° ± 2.8
3	0°	1.08° ± 0.68	1.55° ± 0.05	1.85° ± 1.32	0.88° ± 0.74	4.43° ± 1.00	5.43° ± 2.91
	90°	0 ± 0	0 ± 0	0 ± 0	0 ± 0	0 ± 0	1.35° ± 1.37
4	0°	0 ± 0	0 ± 0	0 ± 0	0.95° ± 0.95	1.10° ± 1.26	1.53° ± 0.80
	90°	0 ± 0	0 ± 0	0 ± 0	0 ± 0	0 ± 0	0 ± 0
5	0°	0 ± 0	0 ± 0	0 ± 0	0 ± 0	0 ± 0	0 ± 0
	90°	0 ± 0	0 ± 0	0 ± 0	0 ± 0	0 ± 0	0 ± 0

At the 1 mm mark, all rods experienced some form of angular deformation. As is consistent with literature, Ti retains less angular deformation than CoCr. The 4.75 Ti, 4.75 CoCr, and 5.5 Ti rod groups no longer experience angular deformation between the 3 and 4 mm mark. The 5.5 CoCr, 6.0 Ti, and 6.0 CoCr rod groups no longer experience angular deformation between the 4 and 5 mm marks.

Roundness

Deformation in the rod via the rod cutter decreased the roundness of the rod closest to the cut location, as seen in Fig. 3.x. At 1 mm, the 6.0 Ti group had an average roundness of 0.976 and the 6.0 CoCr had an average roundness of 0.969. At 1 mm and 2 mm, the 6.0 rod groups mean roundness value was significantly smaller than the 5.5 and 4.75 groups ($p = 0.02$ and $p = 0.04$ respectively). At 3 mm, the groups no longer had statistically different values. All rod groups experienced an increase in roundness over increased distance from the cut end of the rod.

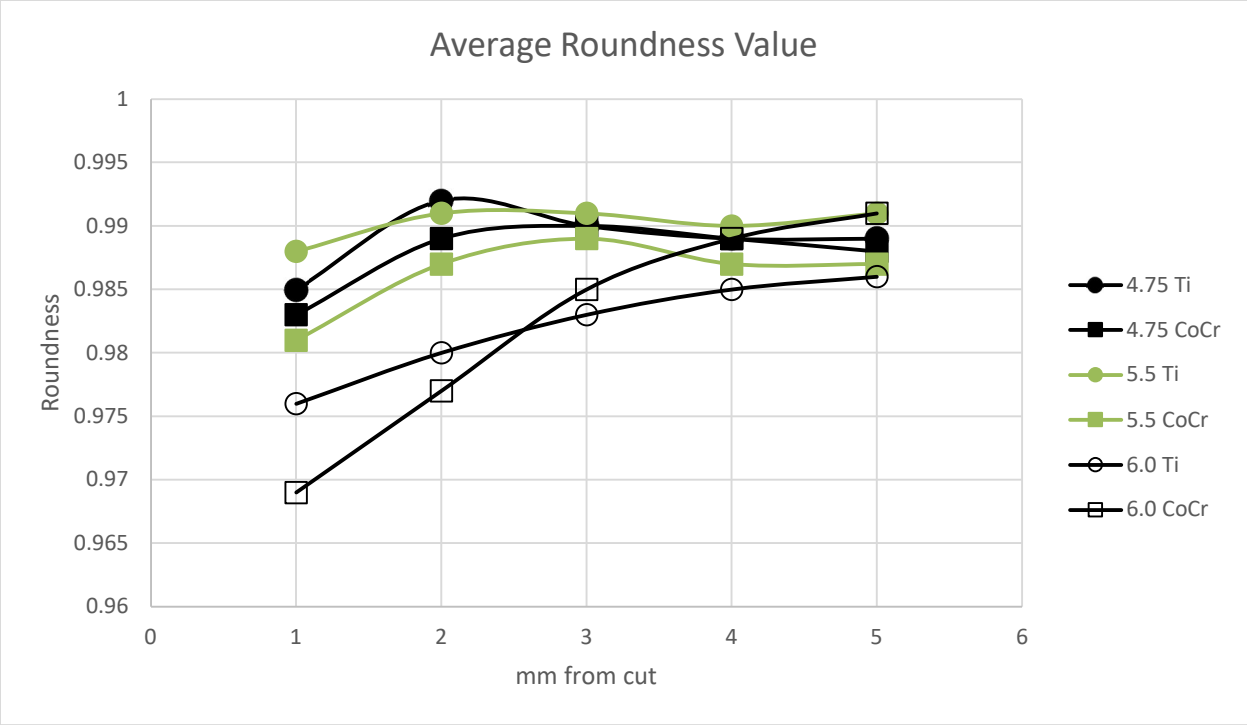

Figure 3.7: Average roundness values of each rod from 1 to 5 mm from the cut edge

Average roundness values are displayed with the standard deviations for each rod group at each measured millimeter (Table 3.2). The 4.75 mm diameter rods experienced small changes in roundness. From 1 mm to 5 mm from the cut end of the rod roundness only increases for the Ti group by 0.004 and 0.005 for the CoCr group. The 5.5 mm diameter Ti group only increases roundness by 0.003, while the 5.5 CoCr group increases by 0.006. The 6.0 mm diameter Ti rod increases roundness by 0.010, while the 6.0 CoCr group increases by 0.022.

Based on the criteria laid out, Table 3.3 provides the minimum distance between the cut end of the rod and the location along the rod that experiences no form of deformation from the rod cutter. For the 4.75 Ti and 5.5 Ti rod groups, 4 millimeters of space are required between the edge of the cut end and where the rod comes in contact with the pedicle screw. For the 4.75

CoCr, 5.5 CoCr, 6.0 Ti, and 6.0 CoCr rod groups, 5 millimeters of space are required between the edge of the cut end and where the rod comes in contact with the pedicle screw.

Table 3.2: Summary Table

Distance from cut end of rod to area of minimal deformation	
4.75 Ti	4mm
4.75 CoCr	5mm
5.5 Ti	4mm
5.5 CoCr	5mm
6.0 Ti	5mm
6.0 CoCr	5mm

Discussion

This study characterized multiple aspects of scoliosis rod deformation that may influence surgeons' clinical decision-making when cutting rods in the intraoperative setting as to how much rod length to leave between the cut end of the rod and the area in which the rod is engaged within the pedicle screw tulip. It was thought that cut angles and roundness were believed to be the most useful values to measure for the deformed ends, as the normal tulip-rod fit assumes fit of an undeformed rod. This deformation may lead to the rod not sitting in the tulip properly and can result in dislodgement or improper correction of the spine (10). In response to this, the aim of this study was to analyze where the deformation ceases along the rod after cutting with the surgical rod cutter.

Cobalt Chrome and Titanium were chosen as the metals to analyze based on common practice standards (6). Typical operating room practice involves shearing of these rods as a method to cut them to size. Cutting metals in this fashion results in deformation of the rod parallel to the pressing direction (12). It has been shown that deformation due to shearing not only changes the shape of the metal but also the material properties (12, 13, 14). When rods are bent, high correction forces are present (15). Additionally, the number of loading cycles the construct can withstand decreases as deformation is introduced (16). Because of this, it is extremely important that this localized area of deformation remain separated from the pedicle screw tulip. Typical locations for rod failure are at the apex of a contoured rod and at the screw-rod interface (7). Instrument failure of this nature is extremely painful and requires repeat surgeries to correct (17).

Table 3.3 displays the distances from edge of the cut to minimal deformation in the rod. Minimal deformation is characterized as no significant difference detected between measured rod segments. Based on results obtained, the 4.75 Ti and 5.5 Ti rod groups require a distance of 4 mm from edge of the cut to pedicle screw contact. The 4.75 CoCr rods show no deformation in the 0° or 90° locations at the 4 mm mark and have a sufficient roundness at the 4 mm mark, but in one trial there was still angular deformation at the 45° location at the 4 mm mark. This is why Table 3.3 shows 5 mm for the 4.75 CoCr rod group. For the 5.5 CoCr, 6.0 Ti, and 6.0 CoCr rod groups, a distance of 5 mm is required from edge of the cut end to pedicle screw contact.

After cutting, the larger diameter rods experienced more deformation than the smaller diameter rods, which did not match the hypothesis of this study. However, this is because cutting larger diameter rods requires more force to break than smaller diameter rods (18). This means a longer duration of time applying forces to these rods, accumulating higher peak forces, which

deforms the larger diameter rods more than the smaller diameter rods. Bodo (19) confirms this in his study where he recorded the peak force on rod cutting handles when cutting different size and metal spinal fusion rods. A 4.75 mm diameter Ti rod recorded a peak force of 250.55 Newtons and a 6.35 mm diameter Ti rod recorded a peak force of 363.95 Newtons. A 6.35 mm CoCr rod recorded a peak force of 396.44 Newtons. CoCr rods of the same size required more force to cut, which stands to be a reason why the CoCr rods generally deformed more than the Ti rods. It has also been observed by Serhan et al that CoCr rods experience more deformation than Ti rods of the same size (20), meaning the deformation pattern between metals and diameters is consistent with existing studies. In the future, our group would like to correlate peak force of the rod cutter with deformation properties for further confirmation of this phenomenon seen.

CoCr rods correct spinal deformities better, compared to stainless steel rods and Ti rods of the same diameter (21, 22). Additionally, rods with larger diameters are associated with a higher degree of spinal correction (23, 24). 6.0 mm CoCr rods may have the best inherent ability to correct the curved spine, however these rods also deform the most from the rod cutter and in the body, post operation (20). The perfect rod – screw combination is yet to be discovered, but new alloys such as molybdenum rhenium (MoRe) have found use in orthopedic implants and demonstrate an improved cyclic life cycle and advantageous biological properties compared to currently used metals (25, 26). A deformation analysis on these new rods would be an interesting project.

Mechanism failure due to insufficient rod roundness has not been specifically researched in this context. Despite extensive literature reviews, no comparable study was found for roundness values, suggesting that an objective baseline value may need to be established. The baseline roundness of the undeformed rods has been set at 0.985 for this paper. This is based off

of the roundness results of the undeformed control rods. If, hypothetically, every undeformed rod had a perfect roundness of 1.0, this baseline is within a 1.5% error. Medtronic's standards call for a diameter tolerance of +/- 0.035mm when machining their spinal fusion rods. On a 6.0 mm rod, this is approximately equivalent to a 0.6% error and on a 4.75 mm rod this is a 0.75% error.

This study had several limitations, one of these being obtaining a true control group. Control measurements for angular deformation and roundness were taken and recorded, however they have not been included in the results section due to a lack of clinical relevancy. Rods assumed to be undeformed are very rare, as most rods are subject to a rod cutter to provide proper fit for the patient (27). Another limitation which should be mentioned is the slight deformation the rod cutter experiences itself after multiple iterations of cutting, however this may be clinically irrelevant as rod cutters are generally used for multiple cases over a longer period of time. The study is also limited by the photography step, as the quality and consistency of the photographs directly impact the quality of the generated 3D model (28). Although efforts were made to mark the servo motor's position for each image set, slight variations in position were inevitable, affecting the rod's position in the images and subsequently influencing the 3D model's accuracy. The camera's attachment to the stand through spinning could have introduced slight deviations. During the photography session, the servo motor was programmed with a consistent rotation, but the analysis of photograph positions in AutoDesk ReCap revealed inconsistent intervals between images. This suggests that the rotation of the servo motor was not perfectly consistent. Software accuracy posed another limitation, with a determined diameter tolerance of +/- 0.05mm based on preliminary study models. This translates to a potential error of approximately 1.05% for a 4.75mm diameter rod and 0.83% for a 6.0mm diameter rod. Consequently, a rough estimation of a 1% error in the measurements taken can be expected.

Lastly, measuring roundness presented challenges as there was no consistent method within Blender to position the particle accurately. To address this, previous screenshots were displayed on a secondary monitor for reference. These limitations highlight the need for further improvements in photography techniques, software accuracy, and roundness measurement methods to enhance the reliability and precision of the study's findings.

Conclusions

An analysis of the deformation found at the end of spinal fusion rod was performed on 4.75, 5.5, and 6.0mm diameter Cobalt Chromium and Titanium rods. It was found that the larger sized diameter rods are subject to more deformation than the smaller diameter rods, and CoCr rods experience more deformation than the Ti rods. In the OR, after cutting the rods, 4 mm of space should be between the edge of the cut rod and where the rod first encounters the pedicle screw for the 4.75 Ti and 5.5 Ti rods. For the 6.0 Ti, 4.75 CoCr, 5.5 CoCr, and 6.0 CoCr rods there should be 5 mm of space between the edge of the cut rod and where the rod first meets the pedicle screw.

References

1. Shakil H., Iqbal Z.A., Al-Ghadir A.H., *Scoliosis: Review of Types of Curves, Etiological Theories and Conservative Treatment*. J Back Musculoskelet Rehabil. 2014. **27**(2): p.111-115.
2. Yaman O., Dalbayrak S., *Idiopathic scoliosis*. Turk Neurosurg. 2014. **24**(5): p. 646-657.
3. Zhang Y.B., Zhang J.G., *Treatment of Early-Onset Scoliosis: Techniques, Indications, and Complications*. Chin Med J (Engl). 2020. **133**(3): p. 351-357.
4. Helenius, I.J., *Standard and Magnetically Controlled Growing Rods for The Treatment Of Early Onset Scoliosis*. Ann Transl Med. 2020. **8**(2): p. 26.
5. Parnell, S.E., Effmann, E.L., Song, K., et al., *Vertical Expandable Prosthetic Titanium Rib (VEPTR): A Review of Indications, Normal Radiographic Appearance and Complications*. Pediatr Radiol. 2015. **45**(4): p. 606–616.
6. Yoshihara, H. *Rods in Spinal Surgery: A Review of The Literature*. The Spine Journal. 2013. **13**(10): p. 1350-1358.
7. Ohrt-Nissen S., Dahl B., Gehrchen M., *Choice of Rods in Surgical Treatment of Adolescent Idiopathic Scoliosis: What Are the Clinical Implications of Biomechanical Properties? - A Review of the Literature*. Neurospine. 2018. **15**(2): p. 123-130.
8. Paik, H., et al., *The Biomechanical Consequences Of Rod Reduction On Pedicle Screws: Should It Be Avoided*?. The Spine Journal. 2013. **13**(11): p. 1617-1626.
9. Abe, Y., Ito, M., Abumi, K., et al., *Scoliosis corrective force estimation from the implanted rod deformation using 3D-FEM analysis*. Scoliosis. 2015. **10** (Suppl 2): S2.
10. Weiss, H.R., Goodall, D., *Rate of Complications in Scoliosis Surgery – A Systematic Review of The Pub Med Literature*. Scoliosis. 2008. **3**: p. 9-9.
11. Paixão, A., Muralha, J., Resende, R. et al. *Close-Range Photogrammetry for 3D Rock Joint Roughness Evaluation*. Rock Mech Rock Eng. 2022. **55**(6): p. 3213–3233.
12. V.M. Segal. *Materials Processing by Simple Shear*. Materials Science and Engineering. 1995. **197**(2): p. 157-164.
13. Fukuda, Y., et al., *Processing of A Low-Carbon Steel by Equal-Channel Angular Pressing*. Acta Materialia. 2002. **50**(6): p. 1359-1368.
14. Wang, J.T., et al., *Microstructure and Properties of a Low-Carbon Steel Processed By Equal-Channel Angular Pressing*. Materials Science and Engineering. 2005. **410**: p. 312-315.
15. Salmingo, R. A., Tadano, S., Fujisaki, K., Abe, Y., Ito, M., *Relationship of Forces Acting on Implant Rods and Degree of Scoliosis Correction.* Clinical Biomechanics. 2013. **28**(2): p. 122-128.
16. Piovesan, A., Berti, F., Villa, T., Pennati, G., La Barbera, L., *Computational and Experimental Fatigue Analysis of Contoured Spinal Rods*. J Biomech Eng. 2019. **141**(4): n. pag.
17. Lonstein, J. E., et al. *Textbook of Scoliosis and Other Spinal Deformities.* Saunders. 1994. p. 515-534.
18. Takase, Y., *Testing and Modeling of Dowel Action for A Post-Installed Anchor Subjected to Combined Shear Force and Tensile Force*. Engineering Structures. 2019. **195**: p. 551-558.
19. Bodo, A., *Design of an In-situ Spinal Rod Cutter for Orthopaedic Surgeons*. 2017. University of Waterloo, Masters Thesis.

20. Serhan, H., et al., *Would CoCr Rods Provide Better Correctional Forces Than Stainless Steel or Titanium for Rigid Scoliosis Curves?*. Journal of Spinal Disorders and Techniques. 2013. **26**(2): p. E70-E74.
21. Lamerain, M., Bachy, M., Delpont, M. et al., *CoCr Rods Provide Better Frontal Correction Of Adolescent Idiopathic Scoliosis Treated By All-Pedicle Screw Fixation*. Eur Spine J. 2014. **23**: p. 1190–1196.
22. Shega, F., et al., *Comparison of Effectiveness between Cobalt Chromium Rods versus Titanium Rods for Treatment of Patients with Spinal Deformity: A Systematic Review and Meta-Analysis.* Advances in Orthopedics. 2020. **2020**: n. pag.
23. Lamartina, C., Petruzzi, M., Macchia, M. et al*., Role of Rod Diameter in Comparison Between Only Screws Versus Hooks and Screws in Posterior Instrumentation of Thoracic Curve in Idiopathic Scoliosis*. Eur Spine J. 2011. **20**(Suppl 1): p. 85–89.
24. Abul-Kasim, K., Karlsson, M.K. & Ohlin, A. *Increased Rod Stiffness Improves The Degree of Deformity Correction By Segmental Pedicle Screw Fixation In Adolescent Idiopathic Scoliosis*. Scoliosis. 2011. **6**: p. 13.
25. Burke, J. F., et al., *Failure in Adult Spinal Deformity Surgery: A Comprehensive Review of Current Rates, Mechanisms, and Prevention Strategies*. Spine. 2022. **47**(19): p 1337-1350.
26. Pedowitz D, Parekh S, Adams S, et al. *Molybdenum Rhenium (MoRe®) as a Biologically Superior Alloy for Foot and Ankle Implants*. Foot & Ankle Orthopaedics. 2018. **3**(3): n. pag.
27. Wang, H., Zhang, J., & Ma, C., *Triple Issues Underlying Lung Injury for Adolescent Idiopathic Scoliosis Surgery*. Lung. 2018. **196**(4): p. 381-382.
28. Jing, X., Zhang, C., Sun, Z., Zhao, G., Wang, Y., *The Technologies of Close-range Photogrammetry and Application in Manufacture*. Proceedings of the 3rd International Conference on Mechatronics, Robotics, and Automation. 2015. p. 988-994.

Chapter 4: Conclusions and Future Work

An analysis of scoliosis rods after cutting with a surgical rod cutter was performed to determine the amount of deformation experienced by each rod. Angular deformation and roundness values were recorded to determine at what point along the rod does the rod no longer experience any sort of deformities. This is important to reduce the chances of instrument failure and repeat surgeries. For the 6.0 Ti rods, 6.0 CoCr, 5.5 CoCr, and 4.75 CoCr rods, deformation stops between the 4.0 mm mark and the 5.0 mm mark. Meaning 5 mm of space should be allowed between the tip of the deformed end of the rod and where the rod first comes into contact with the pedicle screw tulip. For the 5.5 Ti and 4.75 Ti rods, deformation stops between the 3.0 mm mark and the 4.0 mm mark. Meaning, there should be 4 mm between the tip of the deformed end of the rod and where the rod first comes in contact with the pedicle screw tulip. The larger diameter rods experienced more deformation overall. Additionally, the CoCr rods experienced more deformation than the Ti rods of the same diameter.

Overall, the study is limited primarily by the photography step. The quality and consistency of the photographs taken directly influence the quality of the 3D model generated from that set of images. The location where the servo motor should be positioned for each set of images was marked to keep consistent. However, slight variations in position are inevitable which would affect where the rod is in the image, and thus affecting how the 3D model is generated. In addition to that, the camera was tightened to its stand via spinning, which means the camera could have been slightly off angularly as well. The servo motor used in the photography session was programed to rotate every 3.6 degrees every 4 seconds. A feature in the AutoDesk photogrammetry software allows to see the position of each photograph relative to the 3D model itself. After analyzing the position of each image, the distance between the location of each picture is not consistently even.

Typically, there will be two images closer together, and then a slightly larger gap and then two more images closer together. This means that the servo motor was not rotating at perfectly consistent intervals. Software accuracy was also a limitation recognized over the course of the study. Based on several preliminary study models, a software tolerance of +/- 0.05mm was found. On a 4.75 mm diameter rod, this results in a 1.05% error, while on a 6.0 mm diameter rod this results in a 0.83% error. Based on this we can roughly expect a 1% error in the measurements we have taken. The final limitation was based on how roundness was measured. The same size image was taken of the computer screen each time, however, no way to consistently position the location of the particle was found within Blender. To overcome this, previous screenshots were up on a second monitor for reference.

In the future, an investigation on potentially using different tools to cut the rods could be performed to compare the amount of deformation caused by each tool. A different tool may deform the rod less than the current rod cutters being used in practice. In addition to investigation different methods of cutting, analyzing the number of notches or stress risers in the rod after using the French Benders could provide surgeons with more information on the behavior of the deformation along the rod, rather than just the deformation at the top from cutting. Recently, new metals such as molybdenum rhenium (MoRe) have proven useful in orthopedic surgeries and demonstrate advantageous material properties, compared to the CoCr and Ti rods in practice today. An investigation on their utility in spinal fusion surgeries could improve surgical success rate and reduce the number of repeat surgeries due to instrument failure or infection.

Appendix A: Detailed Protocol

Rod Measurement Protocol

1. Take 100 pictures of rod
2. Upload images to computer and filter images
3. Create model in AutoDesk ReCap Photo
4. Export .obj file to Blender
5. Set scale in Blender by measuring base of the rod in 3 spots and measuring actual rod with calipers
6. Rotate rod so that when looking straight onto the rod the left side represents the side with max deformation – this is the 0 degree mark
7. Rotate along all 3 axis to make sure rod is perfectly straight up and down
8. Measure 1 mm down from the top of the rod
9. Use measure tool to trace the slope of the deformation
10. Make a 90 degree cut and extend that out to the other side
11. Make sure the line is 180 degrees
12. Record the measurement
13. Do this until the 5 mm mark
14. Rotate the rod 45 degrees along the z axis
15. Repeat the measurement process starting at step 8

Appendix B: Code

Servo Motor Code

```
// Include the library
#include <Servo.h>

// Create the servo object
Servo myservo;

// Setup section to run once
void setup() {
  myservo.attach(10);       // attach the servo to our servo object

  myservo.write(45);        // Turns the motor in a clockwise motion
}

// Loop to keep the motor turning!
void loop() {
  myservo.write(50);        // Turns the motor in a clockwise motion
  delay(70);               // Determines how long the motor rotates for (in milliseconds)

  myservo.write(90);        // Stops the motor
  delay(4000);              // Stops the motor for 4 seconds allowing me to take picture

}
```

R Code

```
install.packages("rmarkdown")
install.packages("ggplot2")
library(stats)
library(emmeans)
library(ggplot2)

researchdata <- read.csv("C:\\Users\\James\\Documents\\Thesis Research\\Egan_Rstats.csv",
header = T, sep = ",")

researchdata

researchdata$Diameter <- as.factor(researchdata$Diameter)
researchdata$Metal <- as.factor(researchdata$Metal)

angle.0.1 <- aov(researchdata$Angle.0.1 ~ researchdata$Metal * researchdata$Diameter, data =
researchdata)
summary(angle.0.1)

TukeyHSD(angle.0.1)


emmeans(angle.0.1, ~ Metal*Diameter)
fit <- glm(Angle.0.1 ~ Metal * Diameter, data = researchdata)
#emmip(fit, Metal ~ Diameter, CI=T,
 #     xlab = "Diameter (mm)",
  #    ylab = "Angle",
   #   title = "")
emmeans(fit, pairwise ~ Metal | Diameter)$contrasts
emmeans(fit, pairwise ~ Diameter | Metal)$contrasts

angle.0.2 <- aov(researchdata$Angle.0.2 ~ researchdata$Metal * researchdata$Diameter, data =
researchdata)
summary(angle.0.2)

TukeyHSD(angle.0.2)

emmeans(angle.0.2, ~ Metal*Diameter)
fit <- glm(Angle.0.2 ~ Metal * Diameter, data = researchdata)
emmeans(fit, pairwise ~ Metal | Diameter)$contrasts
emmeans(fit, pairwise ~ Diameter | Metal)$contrasts

angle.0.3 <- aov(researchdata$Angle.0.3 ~ researchdata$Metal * researchdata$Diameter, data =
researchdata)
summary(angle.0.3)
```

```
TukeyHSD(angle.0.3)

emmeans(angle.0.3, ~ Metal*Diameter)
fit <- glm(Angle.0.3 ~ Metal * Diameter, data = researchdata)
emmeans(fit, pairwise ~ Metal | Diameter)$contrasts
emmeans(fit, pairwise ~ Diameter | Metal)$contrasts

angle.0.4 <- aov(researchdata$Angle.0.4 ~ researchdata$Metal * researchdata$Diameter, data =
researchdata)
summary(angle.0.4)

TukeyHSD(angle.0.4)

emmeans(angle.0.4, ~ Metal*Diameter)
fit <- glm(Angle.0.4 ~ Metal * Diameter, data = researchdata)
emmeans(fit, pairwise ~ Metal | Diameter)$contrasts
emmeans(fit, pairwise ~ Diameter | Metal)$contrasts

angle.0.5 <- aov(researchdata$Angle.0.5 ~ researchdata$Metal * researchdata$Diameter, data =
researchdata)
summary(angle.0.5)

angle.0.5 <- aov(researchdata$Angle.0.5 ~ researchdata$Metal * researchdata$Diameter, data =
researchdata)
summary(angle.0.5)

TukeyHSD(angle.0.5)

emmeans(angle.0.5, ~ Metal*Diameter)
fit <- glm(Angle.0.5 ~ Metal * Diameter, data = researchdata)
emmeans(fit, pairwise ~ Metal | Diameter)$contrasts
emmeans(fit, pairwise ~ Diameter | Metal)$contrasts


angle.45.1 <- aov(researchdata$Angle.45.1 ~ researchdata$Metal * researchdata$Diameter, data
= researchdata)
summary(angle.45.1)

angle.45.2 <- aov(researchdata$Angle.45.2 ~ researchdata$Metal * researchdata$Diameter, data
= researchdata)
summary(angle.45.2)

angle.45.3 <- aov(researchdata$Angle.45.3 ~ researchdata$Metal * researchdata$Diameter, data
= researchdata)
summary(angle.45.3)
```

```
angle.45.4 <- aov(researchdata$Angle.45.4 ~ researchdata$Metal * researchdata$Diameter, data
= researchdata)
summary(angle.45.4)

angle.45.5 <- aov(researchdata$Angle.45.5 ~ researchdata$Metal * researchdata$Diameter, data
= researchdata)
summary(angle.45.5)

angle.90.1 <- aov(researchdata$Angle.90.1 ~ researchdata$Metal * researchdata$Diameter, data
= researchdata)
summary(angle.90.1)

angle.90.2 <- aov(researchdata$Angle.90.2 ~ researchdata$Metal * researchdata$Diameter, data
= researchdata)
summary(angle.90.2)

angle.90.3 <- aov(researchdata$Angle.90.3 ~ researchdata$Metal * researchdata$Diameter, data
= researchdata)
summary(angle.90.3)

angle.90.4 <- aov(researchdata$Angle.90.4 ~ researchdata$Metal * researchdata$Diameter, data
= researchdata)
summary(angle.90.4)

angle.90.5 <- aov(researchdata$Angle.90.5 ~ researchdata$Metal * researchdata$Diameter, data
= researchdata)
summary(angle.90.5)

roundness.1 <- aov(researchdata$Roundness.1 ~ researchdata$Metal * researchdata$Diameter,
data = researchdata)
summary(roundness.1)

TukeyHSD(roundness.1)

emmeans(roundness.1, ~ Metal*Diameter)
fit <- glm(Roundness.1 ~ Metal * Diameter, data = researchdata)
emmeans(fit, pairwise ~ Metal | Diameter)$contrasts
emmeans(fit, pairwise ~ Diameter | Metal)$contrasts

roundness2 <- aov(researchdata$Roundness.2 ~ researchdata$Metal * researchdata$Diameter,
data = researchdata)
summary(roundness2)

TukeyHSD(roundness2)
```

```
emmeans(roundness2, ~ Metal*Diameter)
fit <- glm(Roundness.2 ~ Metal * Diameter, data = researchdata)
emmeans(fit, pairwise ~ Metal | Diameter)$contrasts
emmeans(fit, pairwise ~ Diameter | Metal)$contrasts

roundness3 <- aov(researchdata$Roundness.3 ~ researchdata$Metal * researchdata$Diameter,
data = researchdata)
summary(roundness3)

TukeyHSD(roundness3)

emmeans(roundness3, ~ Metal*Diameter)
fit <- glm(Roundness.3 ~ Metal * Diameter, data = researchdata)
emmeans(fit, pairwise ~ Metal | Diameter)$contrasts
emmeans(fit, pairwise ~ Diameter | Metal)$contrasts

roundness4 <- aov(researchdata$Roundness.4 ~ researchdata$Metal * researchdata$Diameter,
data = researchdata)
summary(roundness4)

TukeyHSD(roundness4)

emmeans(roundness4, ~ Metal*Diameter)
fit <- glm(Roundness.4 ~ Metal * Diameter, data = researchdata)
emmeans(fit, pairwise ~ Metal | Diameter)$contrasts
emmeans(fit, pairwise ~ Diameter | Metal)$contrasts

roundness5 <- aov(researchdata$Roundness.5 ~ researchdata$Metal * researchdata$Diameter,
data = researchdata)
summary(roundness5)

emmeans(roundness5, ~ Metal*Diameter)
fit <- glm(Roundness.5 ~ Metal * Diameter, data = researchdata)
emmeans(fit, pairwise ~ Metal | Diameter)$contrasts
emmeans(fit, pairwise ~ Diameter | Metal)$contrasts
```

Appendix C: Tables and Graphs

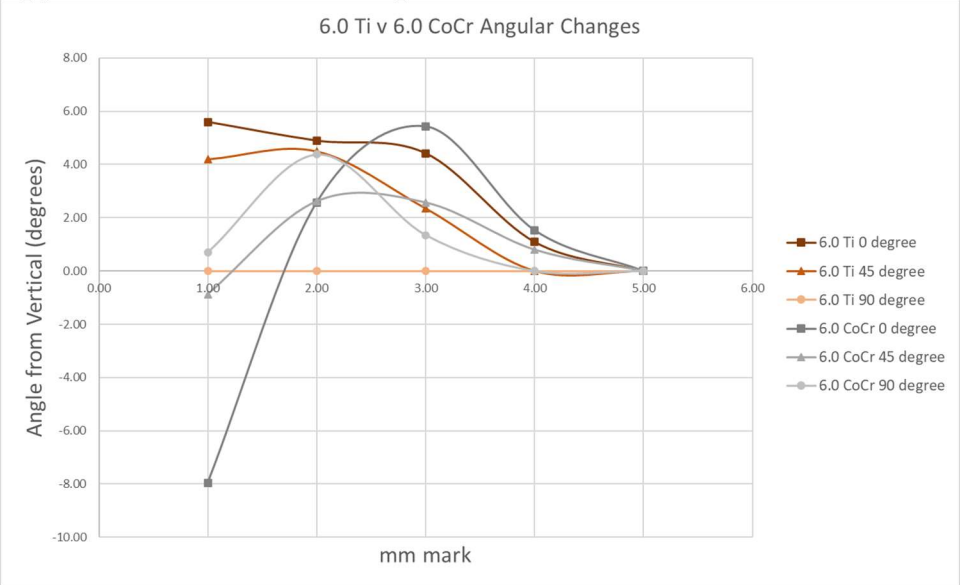

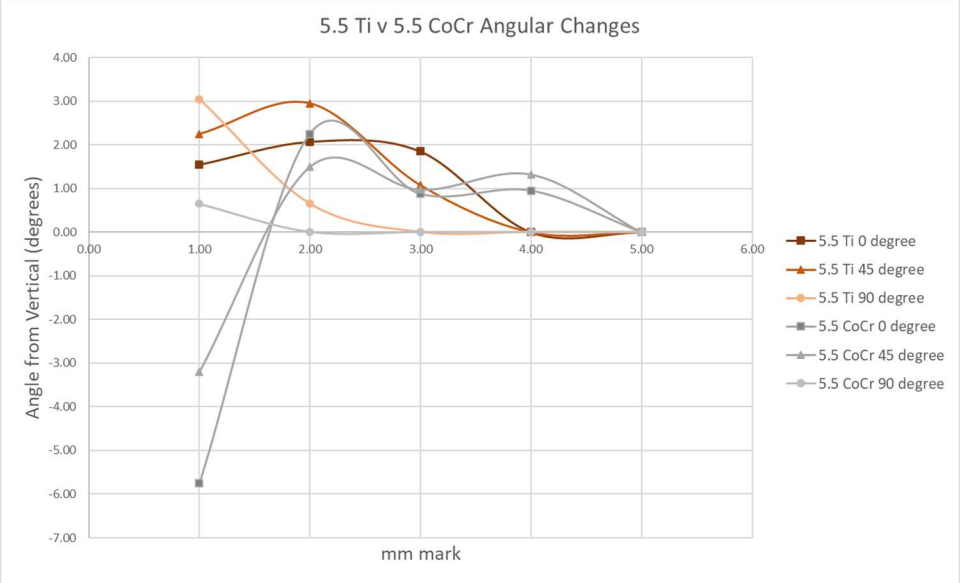

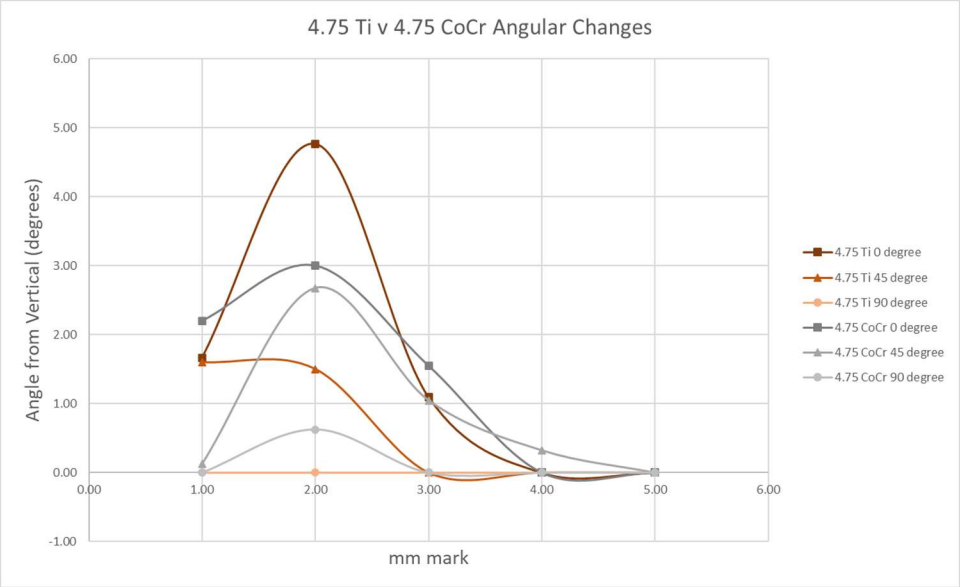

1 mm			
Avg Angle Change (degrees)			
	0	45	90
4.75 Ti	1.7 ± 1.24	2.13 ± 1.37	1.05 ± 1.82
4.75 CoCr	2.2 ± 0.68	0.13 ± 0.22	0 ± 0
5.5 Ti	1.55 ± 0.91	2.25 ± 0.6	3.05 ± 3.15
5.5 CoCr	-5.75 ± 2.46	-3.2 ± 1.3	0.65 ± 0.68
6.0 Ti	5.6 ± 2.81	4.2 ± 1.23	0 ± 0
6.0 CoCr	-7.95 ± 1.24	-0.88 ± 1.74	0.7 ± 1.21

2 mm			
Avg Angle Change (degrees)			
	0	45	90
4.75 Ti	4.1 ± 1.24	1.73 ± 1.96	0 ± 0
4.75 CoCr	3 ± 1.2	2.68 ± 0.55	0.63 ± 1.08

5.5 Ti	2.07 ± 0.65	2.95 ± 1.16	0.65 ± 1.13
5.5 CoCr	2.25 ± 1.51	1.5 ± 1.14	0 ± 0
6.0 Ti	4.9 ± 2.2	4.5 ± 1.76	0 ± 0
6.0 CoCr	2.58 ± 2.4	2.63 ± 0.88	4.38 ± 2.8

3 mm			
Avg Angle Change (degrees)			
	0	45	90
4.75 Ti	1.08 ± 0.68	0 ± 0	0 ± 0
4.75 CoCr	1.55 ± 0.05	1.05 ± 0.55	0 ± 0
5.5 Ti	1.85 ± 1.32	1.08 ± 1.08	0 ± 0
5.5 CoCr	0.88 ± 0.74	0.98 ± 0.67	0 ± 0
6.0 Ti	4.43 ± 1	2.35 ± 2.06	0 ± 0
6.0 CoCr	5.43 ± 2.91	2.58 ± 1.89	1.35 ± 1.37

4 mm			
Avg Angle Change (degrees)			
	0	45	90
4.75 Ti	0 ± 0	0 ± 0	0 ± 0
4.75 CoCr	0 ± 0	0.33 ± 0.56	0 ± 0
5.5 Ti	0 ± 0	0 ± 0	0 ± 0
5.5 CoCr	0.95 ± 0.95	1.33 ± 1.34	0 ± 0
6.0 Ti	1.1 ± 1.26	0 ± 0	0 ± 0
6.0 CoCr	1.53 ± 0.8	0.8 ± 0.48	0 ± 0

5 mm
Avg Angle Change (degrees)

	0	45	90
4.75 Ti	0 ± 0	0 ± 0	0 ± 0
4.75 CoCr	0 ± 0	0 ± 0	0 ± 0
5.5 Ti	0 ± 0	0 ± 0	0 ± 0
5.5 CoCr	0 ± 0	0 ± 0	0 ± 0
6.0 Ti	0 ± 0	0 ± 0	0 ± 0
6.0 CoCr	0 ± 0	0 ± 0	0 ± 0

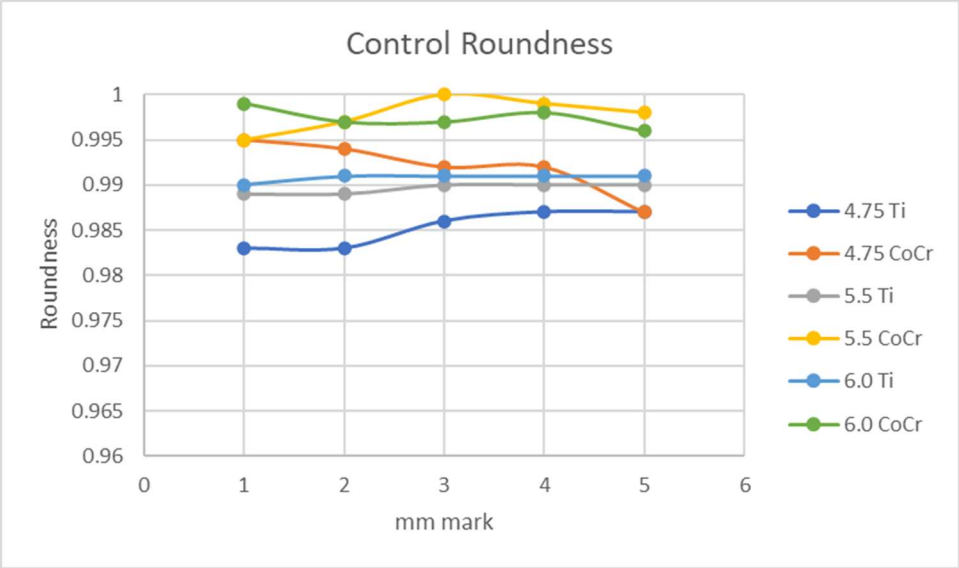

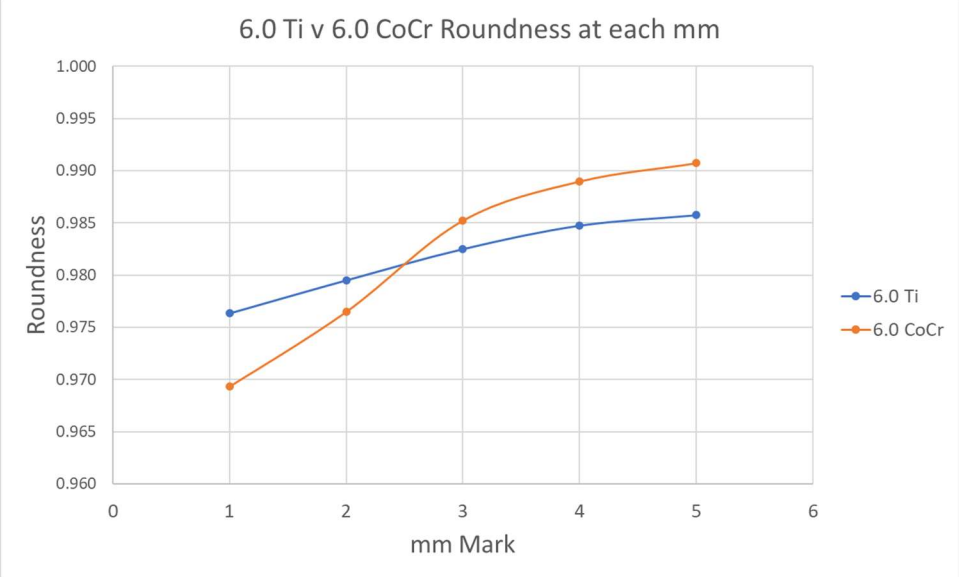


5.5 Ti v 5.5 CoCr Roundness at each mm
Roundness
1.000
0.995
0.990
0.985
0.980
0.975
0.970
0.965
0.960
0
1
2
3
4
5
6
mm Mark
5.5 Ti
5.5 CoCr

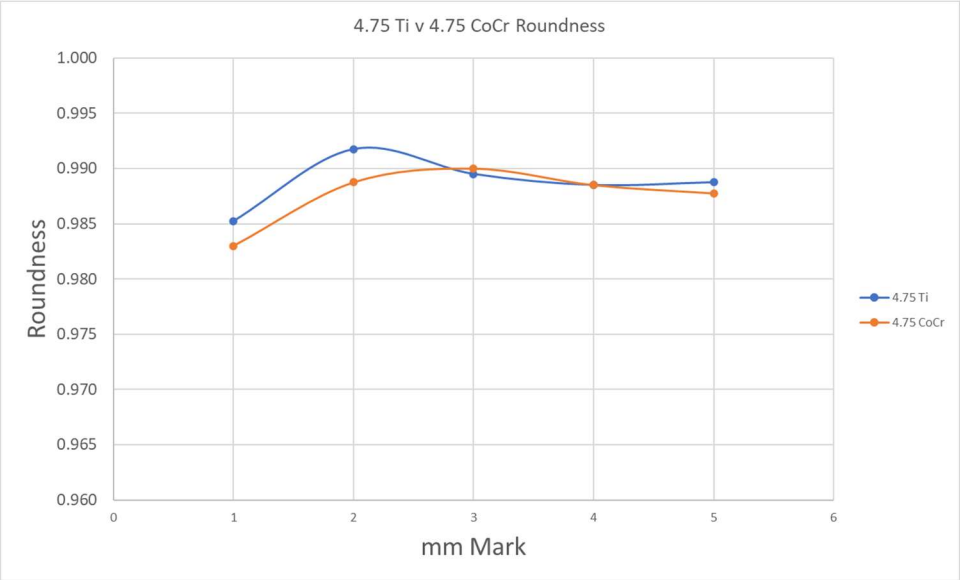
4.75 Ti v 4.75 CoCr Roundness
Roundness
1.000
0.995
0.990
0.985
0.980
0.975
0.970
0.965
0.960
0
1
2
3
4
5
6
mm Mark
4.75 Ti
4.75 CoCr

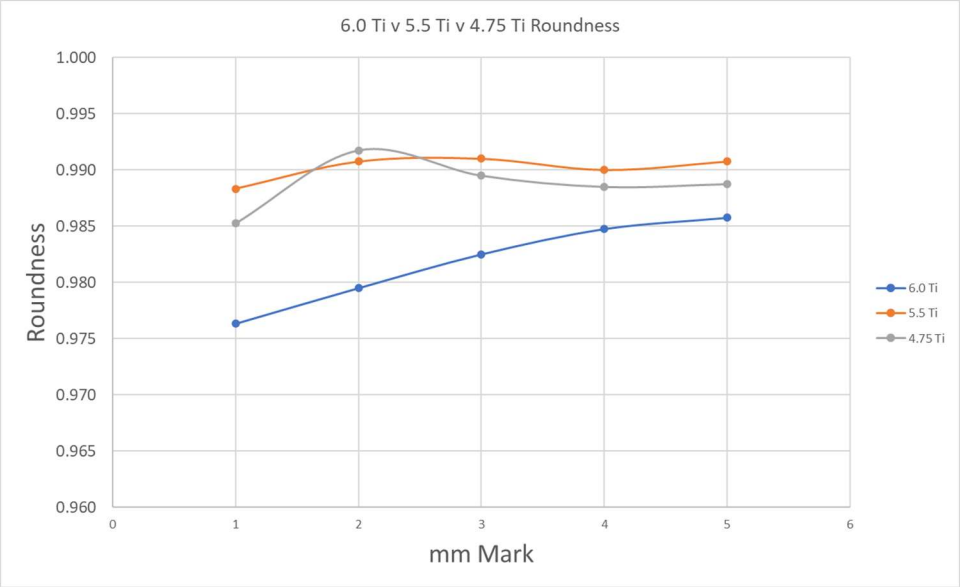
6.0 Ti v 5.5 Ti v 4.75 Ti Roundness
1.000
0.995
0.990
0.985
0.980
0.975
0.970
0.965
0.960
Roundness
0
1
2
3
4
5
6
mm Mark
6.0 Ti
5.5 Ti
4.75 Ti

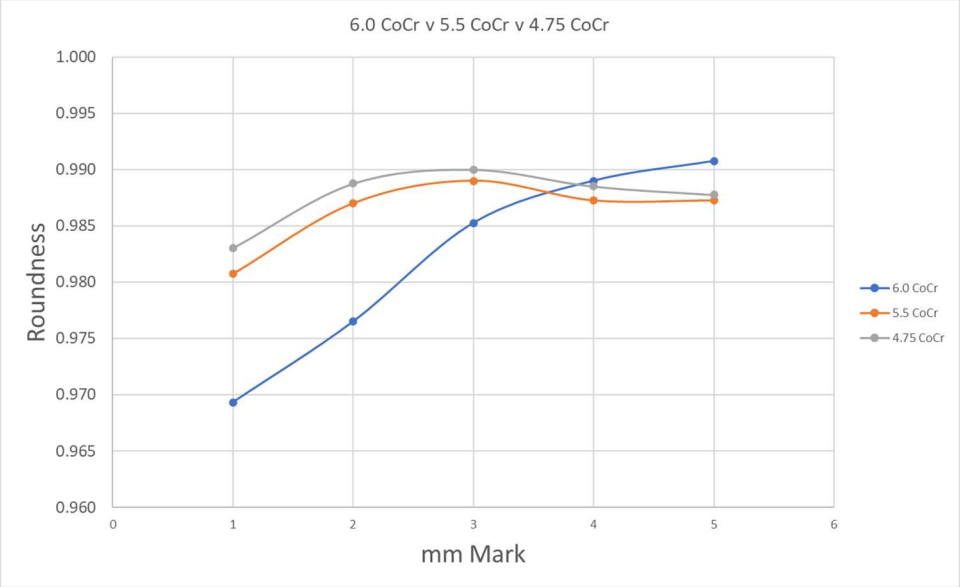
6.0 CoCr v 5.5 CoCr v 4.75 CoCr
1.000
0.995
0.990
0.985
0.980
0.975
0.970
0.965
0.960
Roundness
0
1
2
3
4
5
6
mm Mark
6.0 CoCr
5.5 CoCr
4.75 CoCr